Model for Electron Excitation of the Nucleon. II*

P. L. PRITCHETT† AND J. D. WALECKA
Institute of Theoretical Physics, Department of Physics, Stanford University, Stanford, California 94305
(Received 20 November 1967)

The model of oscillations of the meson field in the nucleon introduced in a previous paper is developed and extended. The model provides a dynamical framework for investigating the electromagnetic properties of the nucleon and gives an excitation spectrum similar to that observed for the nucleon. In this paper we discuss an improved variational solution for the ground-state meson field and the construction of a conserved current. We investigate the problems presented by a fixed-source theory and the linearization of the ϕ^4 theory in constructing this current. Once we have a model for the current, we can calculate all the electromagnetic properties of the nucleon on a consistent basis. We calculate the allowed transverse and Coulomb electron scattering form factors for all the levels of the nucleon up through 2850 MeV, and we compare with existing data wherever possible. We also compare with what is known from phenomenological analysis of photoproduction. Using the magnitude of the ground-state field obtained from a fit to the experimental inelastic form factors, we can compute the anomalous magnetic moment of the nucleon and the pion-nucleon coupling constant. We also use our parameters to investigate the elastic form factors. We show that our model is the appropriate limit of the coupled equations of motion for the meson field and the spin and isospin of the nucleon source. The model is only very crude, but it does indicate some of the interesting things that can be learned from electron excitation of the nucleon.

1. INTRODUCTION

THE construction of very-high-energy electron accelerators makes electron excitation a practical method for investigating the details of the excited states of the nucleon. Existing machines have already been used to study the well known $J^\pi=\frac{3}{2}^+$, $T=\frac{3}{2}$ (1236-MeV) resonance.[1–4] However, the nucleon is now known to have many levels, and an exhaustive study of the higher resonances is being conducted at the Stanford linear accelerator center (SLAC).[5] Important data on these levels are now available from the Cambridge electron accelerator (CEA)[6] and Deutsches electronen-synchrotron (DESY)[7] groups. We indicate in Fig. 1 the numerous states that comprise the low-lying spectrum of the nucleon.[8]

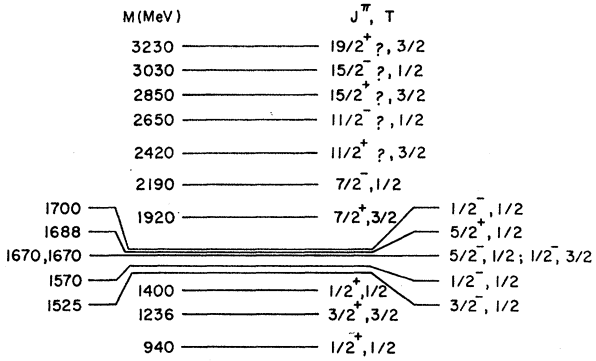

FIG. 1. Low-lying spectrum of the nucleon (see Ref. 8).

From both a theoretical and experimental standpoint one would like to have some idea of what to expect in these experiments. From a theoretical point of view one would at least like to make some predictions before the experiments are completed; from an experimental point of view, estimates of the transition form factors are useful in planning new experiments and in interpreting, understanding, and correlating the data as they accumulate.

The detailed theoretical understanding of these higher excited states requires a theory of strong interactions, and reliable, quantitative calculations are extremely difficult at present. Pending the feasibility of such calculations, one is led to consider models. In the present work we develop further the model of electron excitation introduced by Walecka.[9] This model, which by necessity is very crude, exhibits a level structure quite similar to that shown in Fig. 1 and allows us to calculate the transition form factors. In addition, the model permits us to investigate interrelationships among various electromagnetic properties of the nucleon and its excited levels.

* Research sponsored by the Air Force Office of Scientific Research, Office of Aerospace Research, U. S. Air Force, under AFOSR Contract No. AF49(638)-1389.
† National Science Foundation Predoctoral Fellow.
[1] W. K. H. Panofsky and E. Allton, Phys. Rev. **110**, 1155 (1958).
[2] L. N. Hand, Phys. Rev. **129**, 1834 (1963).
[3] H. L. Lynch, J. V. Allaby, and D. M. Ritson, Phys. Rev. **164**, 1635 (1967); see also, H. L. Lynch, Ph.D. thesis, Stanford University, 1966 (unpublished).
[4] K. Berkelman, in Proceedings of the International Conference on Electromagnetic Interactions at Low and Intermediate Energy, Dubna, USSR, 1967 (unpublished).
[5] SLAC Group A—Proposal 4B, W. Panofsky, D. Coward, H. DeStaebler, J. Litt, L. Mo, R. Taylor, J. Friedman, H. Kendall, L. Van Speybrock, C. Peck, and J. Pine, 1966 (unpublished).
[6] A. A. Cone, K. W. Chen, J. R. Dunning, Jr., G. Hartwig, Norman Ramsey, J. K. Walker, and Richard Wilson, Phys. Rev. **156**, 1490 (1967); Phys. Rev. **163**, 1854 (1967).
[7] F. W. Brasse, T. Engler, E. Ganssauge, and M. Schweizer, in Proceedings of the 1967 International Symposium on Electron and Photon Interactions at High Energies, Stanford Linear Accelerator Center, Stanford, California (to be published); also Deutsches Elektronen-Synchrotron Report No. 67/34, 1967 (unpublished).
[8] A. H. Rosenfeld, A. Barbaro-Galtieri, W. J. Podolsky, L. R. Price, Matts Roos, Paul Soding, W. J. Willis, and C. Wohl, Rev. Mod. Phys. **39**, 1 (1967).
[9] J. D. Walecka, Phys. Rev. **162**, 1462 (1967). Hereafter this article is referred to as I.

As described in I, the starting point for the model is the following pair of observations:

(i) From a dispersion-theory point of view the higher nucleon isobars are very complicated combinations of many-meson states. We might get a first approximation here by going to the other limit and treating the pion field as a classical field, an approximation which should be good when there are many (free) quanta present.

(ii) There should be excitations that correspond to normal-mode oscillations of the pion cloud—similar in spirit to the collective-shape oscillations one has in nuclear physics.[10]

In the rest of this section we discuss briefly how the model has been extended and the new results that have been obtained. In Sec. 2 we present the general formulas for inelastic electron scattering and the inelastic form factors. In Sec. 3 we review the model as developed in I and present an improved variational solution for the ground-state pion field. In Sec. 4 we discuss in detail the construction of a conserved current and gauge invariance and the problems arising in this respect from the use of a fixed source and from the linearization of the theory. In Sec. 5 we give the details of the calculation of the matrix elements and form factors. In Sec. 6 we consider the predictions of the model and compare them with experiment. In Sec. 7 we present a short discussion and summary of the model.

The main extension of the model has been to construct a current $\hat{J}_\mu(\mathbf{x})$ which is conserved: $\partial\hat{J}_\mu(\mathbf{x})/\partial x_\mu=0$. Now the general inelastic electromagnetic vertex is characterized by four reduced matrix elements, or equivalently by the four linear combinations[11]

$$f_\rho=\left(\frac{EE'\Omega^2}{8\pi M^2}\right)^{1/2}\sum_j\left(\frac{2j+1}{2J+1}\right)^{1/2}(j\tfrac{1}{2}1\rho|j1J\tfrac{1}{2}+\rho)\times\langle\pi_R J\|\hat{\mathbf{J}}(0)\|q^*\pi j\rangle, \quad (1.1)$$

with $\rho=\pm1, 0$, and

$$f_c=(EE'\Omega^2/8\pi M^2)^{1/2}\langle\pi_R J\|\hat{J}_0(0)\|q^*\pi J\rangle. \quad (1.2)$$

In these expressions E and E' are the initial and final target energies, M is the isobar mass, Ω is the normalization volume, $\hat{J}_\mu(0)=(\hat{\mathbf{J}}(0),i\hat{J}_0(0))$ is the electromagnetic current operator taken at the origin, and J^{π_R} is the angular momentum and parity of the isobar. In the rest frame of the isobar one has

$$q_\mu\equiv(\mathbf{q}^*,iq_0). \quad (1.3)$$

Current conservation provides one relation among these four quantities, and it simply eliminates f_0:

$$f_0=(q_0/q^*)f_c. \quad (1.4)$$

In our model we calculate $|f_+|^2$, $|f_-|^2$, and $|f_c|^2$ or, equivalently, the matrix elements of the transition multipoles $\hat{T}_{LM}^{\rm el}(q^*)$, $\hat{T}_{LM}^{\rm mag}(q^*)$, and $\hat{M}_{LM}^{\rm Coul}(q^*)$. There is no longitudinal term corresponding to f_0. In general, the three multipole operators $\hat{T}_{LM}^{\rm el}$, $\hat{T}_{LM}^{\rm mag}$, and $\hat{M}_{LM}^{\rm Coul}$ are independent. But for the normal parity transitions there is a relation well known in nuclear physics[10] between the matrix elements of $\hat{T}_{LM}^{\rm el}$ and $\hat{M}^{\rm Coul}$ in the long-wavelength limit:

$$|\langle f\|\hat{T}_L^{\rm el}\|i\rangle|^2\underset{q^*\to0}{\approx}\left(\frac{q_0}{q^*}\right)^2\left(\frac{L+1}{L}\right)|\langle f\|\hat{M}_L^{\rm Coul}\|i\rangle|^2. \quad (1.5)$$

In our calculations we use current conservation to replace $\nabla\cdot\hat{\mathbf{J}}$ by $-\dot{\rho}$ in the expression for $\hat{T}_{LM}^{\rm el}$. Consequently, the relation (1.5) is automatically satisfied in our model.[12]

A second extension has been to find a better variational solution for the ground-state pion field. The variational form contains three parameters rather than one, as was the case in I. At large distances the variational solution reduces to the Yukawa tail, and we can identify the renormalized pion-nucleon coupling constant $f_{\pi N}^2$. It should be noted that our model has a finite coupling-constant renormalization since $G_{\pi N}$ is different from G, where G is the coupling constant that enters into the original Hamiltonian.

We give predictions for the transverse and Coulomb form factors for all the allowed levels up to the $J^\pi=\frac{15}{2}+$ (?), $T=\frac{3}{2}$ (2850-MeV) level. (Allowed levels are those that can be connected to the ground state of the nucleon by the operation of a single creation or destruction operator.) In addition, we give predictions for all the background states which are supposed to resonate in the region of each main level. Taking the limit $q_\mu^2\to0$, we can compare our predictions with the various phenomenological analyses of photoproduction[13,14] which have been carried out in the higher resonance regions. The relation between the usual photoproduction amplitudes and the multipole operators used in the present work is derived in Appendix A.

The current in our model has a ground-state expectation value proportional to the square of the ground-state pion field, and so we can compute the anomalous isovector magnetic moment of the nucleon. We also calculate the elastic form factors and give values for the root-mean-square radius for the charge and magnetic moment of the nucleon.

2. ELECTRON SCATTERING

We give here a brief review of the theory of electron scattering. We consider the case where only the final

[10] T. deForest, Jr., and J. D. Walecka, Advan. Phys. **15**, 1 (1966).

[11] J. D. Bjorken and J. D. Walecka, Ann. Phys. (N. Y.) **38**, 35 (1966).

[12] Note, therefore, that all the *general* properties of the theory coming from current conservation, or equivalently gauge invariance, are actually built into the calculation at the start.

[13] R. Walker (private communication); and (to be published).

[14] Y. C. Chau, Norman Dombey, and R. G. Moorhouse, Phys. Rev. **163**, 1632 (1967).

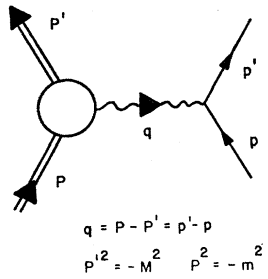

FIG. 2. Kinematics for inelastic electron scattering in the one-photon-exchange approximation.

electron is detected as in most of the experiments performed so far and in those being carried out at SLAC.[5] Bjorken and Walecka[11] have given a relativistically covariant analysis of the process of electron excitation of the nucleon and have discussed all that can be said about the transition form factors on general grounds. They have also shown the relation to photoexcitation of the nucleon resonances. We summarize their results.

Figure 2 illustrates the kinematics of electron scattering in the one-photon-exchange (OPE) approximation. The angular momentum analysis is best carried out in the rest frame of the final isobar because one then has an eigenstate of angular momentum and parity. The electromagnetic vertex is characterized by the four quantities $f_\pm, f_0, f_c$ given in Eqs. (1.1) and (1.2). Current conservation eliminates f_0 in terms of f_c [see Eq. (1.4)]. The electron scattering cross section in the laboratory is then shown to be (we set $m_e=0$)

$$\left(\frac{d\sigma}{d\Omega}\right)_{\text{lab}}=\frac{\alpha^2\cos^2(\frac{1}{2}\theta)}{4\epsilon^2\sin^4(\frac{1}{2}\theta)[1+(2\epsilon/m)\sin^2(\frac{1}{2}\theta)]}\left\{\frac{q^4}{q^{*4}}|f_c|^2+\left(\frac{q^2}{2q^{*2}}+\frac{M^2}{m^2}\tan^2(\tfrac{1}{2}\theta)\right)[|f_+|^2+|f_-|^2]\right\}. \quad (2.1)$$

In this expression ϵ is the initial electron energy, θ is the electron scattering angle, m is the nucleon mass, and $q^2=q_\mu{}^2$ is the invariant four-momentum transfer. We see that electron scattering measures two independent combinations of form factors, the Coulomb and transverse form factors. These may be separated experimentally by keeping q^2 and the energy loss $-q_0=\epsilon-\epsilon'$ fixed and varying θ or by working at $\theta=180°$, where only the transverse contribution remains. The transverse form factor can also be measured *at one momentum transfer*, namely $q_\mu{}^2=0$, or

$$q^*_{\text{threshold}}=(M^2-m^2)/2M; \quad (2.2)$$

in photoexcitation

$$\int_{\text{lab; over resonance}}\sigma_\gamma(\omega)d\omega=\frac{4\pi^2\alpha}{M^2-m^2}\frac{M^2}{m}\times[|f_+|^2+|f_-|^2]_{q^2=0}. \quad (2.3)$$

Thus with electron scattering, we can add a new dimension onto the photon problem. In addition, there is also the possibility of direct Coulomb excitation.

Detailed properties of the form factors $f_c, f_\pm$ are highly model-dependent. However, in the limit $q^*\to 0$ (which implies $-q_0\to M-m$) the form factors have simple threshold behaviors:

(1) Normal parity transitions $\frac{1}{2}^+\to\frac{3}{2}^-,\frac{5}{2}^+,\cdots$

$$f_c\sim(q^*)^{J-1/2},$$
$$f_\pm\sim(q^*)^{J-3/2}.$$

(2) Abnormal parity transitions $\frac{1}{2}^+\to\frac{1}{2}^-,\frac{3}{2}^+,\frac{5}{2}^-,\cdots$

$$f_c\sim(q^*)^{J+1/2},$$
$$f_\pm\sim(q^*)^{J-1/2}.$$

Experimentally, only spacelike momentum transfers $[q^2\geq 0]$ are available, and it is not clear whether the threshold behavior still persists in this region since this implies a minimum three-momentum transfer

$$q^*\geq q^*_{\text{threshold}}=(M^2-m^2)/2M.$$

This is an interesting question on which we would like our model to shed some light.

For the normal parity transitions there is an additional relation between f_c and $f_\pm$ valid near threshold:

$$\frac{|f_+|^2+|f_-|^2}{|f_c|^2}\underset{q^*\to 0}{\approx}\left(\frac{J+\frac{1}{2}}{J-\frac{1}{2}}\right)\left(\frac{q_0}{q^*}\right)^2, \quad (2.4)$$

which is just Eq. (1.5).

With a well-localized source, as is the case in nuclear physics, one can give expressions for the transition form factors in terms of the Fourier transform of the transition charge and current densities[10]:

$$|f_c|^2=\frac{4\pi}{2J_i+1}\sum_{L=0}^{\infty}|\langle J_f\|\hat{M}_L{}^{\text{Coul}}(q^*)\|J_i\rangle|^2, \quad (2.5)$$

$$|f_+|^2+|f_-|^2=\frac{4\pi}{2J_i+1}\sum_{L=1}^{\infty}[|\langle J_f\|\hat{T}_L{}^{\text{el}}(q^*)\|J_i\rangle|^2+|\langle J_f\|\hat{T}_L{}^{\text{mag}}(q^*)\|J_i\rangle|^2]; \quad (2.6)$$

$$\hat{M}_{LM}{}^{\text{Coul}}(q^*)=\int j_L(q^*x)Y_{LM}(\Omega_x)\hat{\rho}(\mathbf{x})d\mathbf{x}, \quad (2.7)$$

$$\hat{T}_{LM}{}^{\text{el}}(q^*)=(1/q^*)\int[\nabla\times\{j_L(q^*x)\mathcal{Y}_{LL1}{}^M(\Omega_x)\}]\cdot\hat{\mathbf{J}}(\mathbf{x})d\mathbf{x}, \quad (2.8)$$

$$\hat{T}_{LM}{}^{\text{mag}}(q^*)=\int[j_L(q^*x)\mathcal{Y}_{LL1}{}^M(\Omega_x)]\cdot\hat{\mathbf{J}}(\mathbf{x})d\mathbf{x}, \quad (2.9)$$

where the nuclear electromagnetic current operator is

$$\hat{J}_\mu=(\hat{\mathbf{J}}(\mathbf{x}),i\hat{\rho}(\mathbf{x})), \quad (2.10)$$

and $\mathcal{Y}_{LL1}{}^M$ are vector spherical harmonics,[15] which can be written as

$$\mathcal{Y}_{LL1}{}^M(\Omega_x)=-i[L(L+1)]^{-1/2}(\mathbf{x}\times\nabla)Y_{LM}(\Omega_x). \quad (2.11)$$

[15] We use the angular momentum notation of A. R. Edmonds, *Angular Momentum in Quantum Mechanics* (Princeton University Press, Princeton, N. J., 1957).

Integrating by parts and using $\nabla\times\mathbf{x}=0$, we can write (2.9) as

$$\hat{T}_{LM}^{\rm mag}(q^*)=\frac{i}{[L(L+1)]^{1/2}}\int j_L(q^*x)Y_{LM}(\Omega_x)\times(\mathbf{x}\cdot[\nabla\times\hat{\mathbf{J}}(\mathbf{x})])d\mathbf{x}, \quad (2.12)$$

and (2.8) as

$$\hat{T}_{LM}^{\rm el}(q^*)=\frac{1}{iq^*}\frac{1}{[L(L+1)]^{1/2}}\int j_L(q^*x)Y_{LM}(\Omega_x)\times[\nabla\cdot[\mathbf{x}\times(\nabla\times\hat{\mathbf{J}}(\mathbf{x}))]]d\mathbf{x}. \quad (2.13)$$

Expanding the divergence term we can finally write

$$\hat{T}_{LM}^{\rm el}(q^*)=\frac{1}{iq^*}\frac{1}{[L(L+1)]^{1/2}}\int[(\nabla\cdot\hat{\mathbf{J}}(\mathbf{x}))(1+\mathbf{x}\cdot\nabla)\times j_L(q^*x)Y_{LM}(\Omega_x)-q^{*2}j_L(q^*x)Y_{LM}(\Omega_x)\mathbf{x}\cdot\hat{\mathbf{J}}(\mathbf{x})]d\mathbf{x}. \quad (2.14)$$

When we evaluate $\hat{T}_{LM}^{\rm el}$, we shall replace $\nabla\cdot\hat{\mathbf{J}}$ by $-\dot{\rho}$. Our model will thus *automatically* satisfy the threshold relations depending on current conservation.

What we shall do when we make our model is use the form of the cross section of Eq. (2.1), which was derived in a Lorentz-invariant way and which has the relativistically correct kinematic factor extracted. We shall then use the above expressions, which are applicable to a fixed-source theory, to evaluate the transition matrix elements. The transition multipoles will be evaluated for a momentum transfer q^*. For a fixed-source theory there is no ambiguity; when the source recoils, however, there is no unique prescription. We use q^* since the original analysis[11] was carried out most directly in the rest frame of the final isobar. We are thus evaluating the kinematic factors correctly and neglecting recoil only in the transition matrix elements. Such a treatment must break down at very large momentum transfers, and our results there are at best qualitative. A better treatment, while greatly desirable, is very difficult [witness the situation in the much simpler case of elastic scattering from the deuteron at large momentum transfers].

3. REVIEW OF THE MODEL

As in I, we start from the following Hamiltonian for a symmetric, pseudoscalar-meson field[16]:

$$H=\frac{1}{2}\int d\mathbf{x}(\dot{\phi}_\alpha\dot{\phi}_\alpha+\nabla\phi_\alpha\cdot\nabla\phi_\alpha+\mu^2\phi_\alpha\phi_\alpha)+\tfrac{1}{4}\lambda\int d\mathbf{x}(\phi_\alpha\phi_\alpha)^2-\tfrac{1}{2}\beta\int_0^a d\mathbf{x}\,\phi_\alpha\phi_\alpha+(G/2m)\int d\mathbf{x}\,\tau_\alpha(\boldsymbol{\sigma}\cdot\nabla\phi_\alpha)S(x). \quad (3.1)$$

[16] W. Pauli, *Meson Theory of Nuclear Forces* (Interscience Publishers, Inc., New York, 1946).

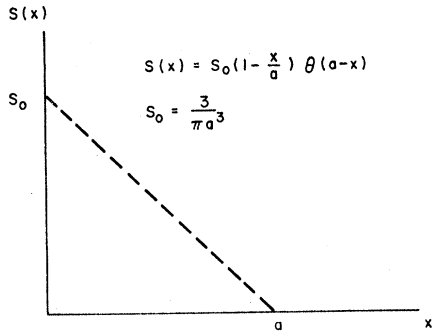

FIG. 3. Assumed form of $S(x)$, the nucleon source distribution.

α is an isotopic spin index which runs from 1 to 3, $S(x)$ is the nucleon source distribution function, and λ, β, and G are coupling constants. $\boldsymbol{\sigma}$ and $\boldsymbol{\tau}$ are the usual Pauli matrices.

To make the Hamiltonian a little more realistic, we have included a phenomenological attractive potential scattering term with strength β inside the core region. This is to represent particle exchanges such as vector mesons, baryon pairs, etc. We have also assumed a repulsive ($\lambda>0$) ϕ^4 meson-meson interaction for reasons which will become apparent. To simplify the problem still further, we assume that $S(x)$ has a uniform gradient out to radius a, as shown in Fig. 3. Thus we write

$$S(x)=(3/\pi a^3)(1-x/a)\theta(a-x). \quad (3.2)$$

Since we are interested in the oscillations of the pion cloud, we neglect the dynamics of the spin and isospin of the nucleon source. Thus we assume that

$$\dot{\sigma}_\alpha\approx 0, \quad \dot{\tau}_\alpha\approx 0. \quad (3.3)$$

(We discuss this assumption further in Sec. 4 and Appendix B.) $\boldsymbol{\sigma}$ and $\boldsymbol{\tau}$ are included so that we have the correct over-all transformation properties.

To find the ground state of the Hamiltonian, we minimize H with respect to a time-independent ϕ_0^α: $\delta H/\delta\phi_0^\alpha=0$. This leads to the following nonlinear differential equation:

$$[\nabla^2-\mu^2-\lambda\phi_0^\beta\phi_0^\beta+\beta\theta(a-x)]\phi_0^\alpha(\mathbf{x})=-(G/2m)\tau^\alpha(\boldsymbol{\sigma}\cdot\nabla)S(x). \quad (3.4)$$

We are interested in excitations of the system, and so we expand the pion field about its ground state:

$$\phi^\alpha(\mathbf{x},t)=\phi_0^\alpha(\mathbf{x})+\eta^\alpha(\mathbf{x},t). \quad (3.5)$$

Inserting this expansion in H and using the differential equation satisfied by $\phi_0^\alpha(\mathbf{x})$, we arrive at the following equation for η^α:

$$[\nabla^2-\partial^2/\partial t^2-\mu^2+\beta\theta(a-x)-\lambda(\phi_0^\beta\phi_0^\beta)]\eta^\alpha=\lambda\eta^\beta[\phi_0^\alpha\phi_0^\beta+\phi_0^\beta\phi_0^\alpha]. \quad (3.6)$$

The ground-state pion field thus creates an additional

potential in which the field can oscillate.[17] We can expand the field η^α in the same manner as is done for the free-meson field,

$$\eta^\alpha(\mathbf{x},t)=\sum_{nlm}\frac{1}{[2\omega_{nl}]^{1/2}}[c_{nlm}{}^\alpha\eta_{nlm}(\mathbf{x})e^{-i\omega_{nl}t} +c_{nlm}{}^{\alpha\dagger}\eta_{nlm}{}^\dagger(\mathbf{x})e^{i\omega_{nl}t}]. \quad (3.7)$$

As shown in I, we can interpret $c_{nlm}{}^{\alpha\dagger}$ and $c_{nlm}{}^\alpha$ as the creation and destruction operators for the normal-mode excitations of the pion field. We impose the commutation rules

$$[c_{nlm}{}^\alpha, c_{n'l'm'}{}^{\alpha'\dagger}]=\delta_{\alpha\alpha'}\delta_{nn'}\delta_{ll'}\delta_{mm'} \quad (3.8)$$

in order to quantize these excitations.

We can try to get a crude solution to the nonlinear differential Eq. (3.4) by using the following three-parameter variational form:

$$\begin{aligned}&\phi_0{}^\alpha(\mathbf{x})=\tau^\alpha(\boldsymbol{\sigma}\cdot\hat{x})\phi_0(x),\\ &\phi_0(x)=c, \qquad x<a\\ &\quad=c\left[\frac{e^{-\rho(x-a)}}{x/a}(1-\epsilon)+\frac{e^{-\mu(x-a)}}{x/a}\epsilon\right], \quad x>a.\end{aligned} \quad (3.9)$$

c, ρ, and ϵ are the parameters to be varied. At large distance the solution for $\phi_0{}^\alpha$ must reduce to the Yukawa tail arising from the (OPE) pole;

$$\phi_0{}^\alpha(\mathbf{x})\underset{x\to\infty}{\longrightarrow}\frac{\mu}{2m}\frac{G_{\pi N}}{4\pi}\tau^\alpha\boldsymbol{\sigma}\cdot\hat{x}\frac{e^{-\mu x}}{x}. \quad (3.10)$$

We thus obtain the following expression for the renormalized pion-nucleon coupling constant:

$$f_{\pi N}{}^2\equiv(1/4\pi)(\mu/2m)^2G_{\pi N}{}^2=4\pi\epsilon^2(ca)^2e^{2\mu a}, \quad (3.11)$$

which depends on two of the variational parameters. Thus our model has a finite renormalization with $G_{\pi N}\neq G$, where G is the coupling constant in the Hamiltonian (3.1). Note that we assume for simplicity that ϕ_0 is constant for $x<a$.

The equation for η^α then takes the form

$$[\nabla^2+k^2-v(x)]\eta^\alpha(\mathbf{x})=0, \quad (3.12)$$

where

$$\begin{aligned}&v(x)=-\beta+5\lambda c^2, \qquad x<a\\ &\quad=5\lambda c^2\left[\frac{e^{-\rho(x-a)}}{x/a}(1-\epsilon)+\frac{e^{-\mu(x-a)}}{x/a}\epsilon\right]^2, \quad x>a\end{aligned} \quad (3.13)$$

and where k is defined by

$$\omega^2-\mu^2=k^2. \quad (3.14)$$

[17] This approach was first used in another context by L. I. Schiff, Phys. Rev. 84, 1 (1951). See also D. Yennie, *ibid.* 88, 527 (1952) for a criticism of treating a $\lambda\phi^4$ theory as a classical field theory when λ or ϕ are large. He points out that quantum fluctuations then become large. This point is discussed in detail in I.

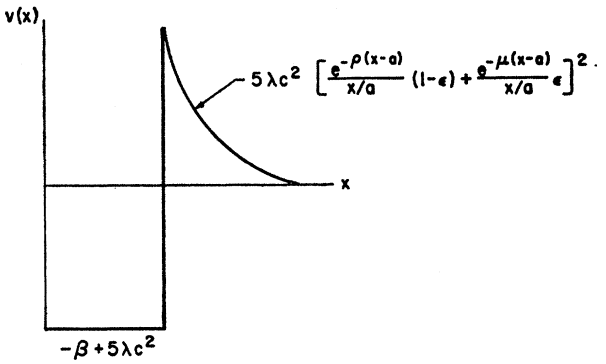

FIG. 4. The potential $v(x)$ in $[\nabla^2+k^2-v(x)]\eta=0$.

We thus have to solve a Schrödinger equation with the potential illustrated in Fig. 4. The repulsive meson-meson interaction gives us an additional barrier which, when added to the centrifugal barrier $l(l+1)/a^2$, allows us to have sharp resonances high in the continuum. Assuming that we can extend the barrier to infinity, we can immediately write down the solutions for η:

$$\begin{aligned}&\eta_{nlm}(\mathbf{x})=R_{nl}(x)Y_{lm}(\Omega_x),\\ &R_{nl}(x)=\left[\frac{2}{a^3j_{l+1}{}^2(X_{nl})}\right]^{1/2}j_l(K_{nl}x),\end{aligned} \quad (3.15)$$

where $X_{nl}\equiv K_{nl}a$ and $j_l(X_{nl})=0$. k_{nl} and K_{nl} are related by

$$k_{nl}{}^2=(1/a^2)[X_{nl}{}^2-\beta a^2+5\lambda c^2a^2]. \quad (3.16)$$

The resulting spectrum is shown in Fig. 5 for the following choice of parameters:

$$\begin{aligned}\mu a&=1,\\ \beta a^2-5\lambda c^2a^2&=16,\\ 5\lambda c^2a^2&=40.\end{aligned} \quad (3.17)$$

The last relation gives a barrier which is high enough so that the states we are interested in will show up as

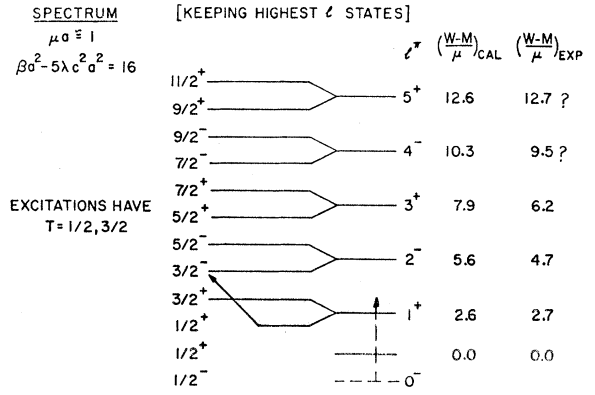

FIG. 5. Spectrum for the choice of parameters in the text: $\mu a=1$, $\beta a^2-5\lambda c^2a^2=16$.

resonances as discussed in I, but the exact value here is not very well determined. We note the following features:

(i) Coupling the spin of the nucleon to the meson excitations and keeping just the highest l states as we go up in energy (these are the states which will have a large enough barrier to show up as resonances), we get a spectrum very similar to that observed for the nucleon.

(ii) The excitations have $T=\frac{1}{2}$ and $\frac{3}{2}$ since we couple the isovector excitations to the isospin of the nucleon core. We therefore appear to have a doubling of states compared with experiment, but it is probably too strong a statement to assume that our β is independent of spin and isospin. Notice, however, that every level which has been experimentally identified for the nucleon has its counterpart on this figure.

(iii) There is a low-lying s-wave state, but its exact position is, of course, very sensitive to what goes on in the inner region of the nucleon. The low-lying $\frac{1}{2}^+$ state will get pushed up by its interaction with the ground state.

We can now proceed with the variational calculation for the ground-state pion field. Using the result

$$\nabla^2[(\boldsymbol{\sigma}\cdot\hat{x})\phi_0(x)]=(\boldsymbol{\sigma}\cdot\hat{x})\left(\frac{1}{x}\frac{d^2}{dx^2}\mathbf{x}-\frac{2}{x^2}\right)\phi_0(x), \quad (3.18)$$

we can write H for the ground state $\phi_0{}^\alpha$ as

$$H_0=H_{\text{core}}+H_{\text{tail}}, \quad (3.19)$$

where

$$H_{\text{core}}=\frac{3}{2}\int_0^a d\mathbf{x}[\nabla\phi_0\cdot\nabla\phi_0+(2/x^2)\phi_0{}^2+\mu^2\phi_0{}^2 +\tfrac{3}{2}\lambda\phi_0{}^4-\beta\phi_0{}^2+(3G/\pi ma^4)\phi_0], \quad (3.20)$$

and

$$H_{\text{tail}}=\frac{3}{2}\int_a^\infty d\mathbf{x}[\nabla\phi_0\cdot\nabla\phi_0+(2/x^2)\phi_0{}^2 +\mu^2\phi_0{}^2+\tfrac{3}{2}\lambda\phi_0{}^4]. \quad (3.21)$$

For $x<a$, $\phi_0=c$. Thus,

$$H_{\text{core}}=(2\pi/a)c^2a^2[6+\mu^2a^2+\tfrac{3}{2}\lambda c^2a^2 -\beta a^2+3G/\pi maca]. \quad (3.22)$$

Note that H_{core} does not depend on either ρ or ϵ. Using the explicit form of ϕ_0 for $x>a$, we have

$$H_{\text{tail}}=(6\pi/a)c^2a^2[\tfrac{3}{2}\lambda c^2a^2A_4\epsilon^4+\tfrac{3}{2}\lambda c^2a^2A_3\epsilon^3 +(B_2+\tfrac{3}{2}\lambda c^2a^2A_2)\epsilon^2+(B_1+\tfrac{3}{2}\lambda c^2a^2A_1)\epsilon+B_0 +\tfrac{3}{2}\lambda c^2a^2I(4\rho a)], \quad (3.23)$$

with

$$\begin{aligned}
A_4&=I(4\rho a)-4I(3\rho a+\mu a)+6I(2\rho a+2\mu a)\\
&\quad -4I(\rho a+3\mu a)+I(4\mu a),\\
A_3&=-4I(4\rho a)+12I(3\rho a+\mu a)-12I(2\rho a+2\mu a)\\
&\quad +4I(\rho a+3\mu a),\\
A_2&=6I(4\rho a)-12I(3\rho a+\mu a)+6I(2\rho a+2\mu a),\\
A_1&=-4I(4\rho a)+4I(3\rho a+\mu a),\\
B_2&=(1/2\rho a)[\mu^2a^2+\rho^2a^2+2\rho a]+2I(2\rho a)\\
&\quad -[2/(\rho+\mu)a][\mu^2a^2+\rho\mu a^2+(\rho+\mu)a]\\
&\quad -4I(\rho a+\mu a)+(1+\mu a)+2I(2\mu a),\\
B_1&=-(1/\rho a)[\mu^2a^2+\rho^2a^2+2\rho a]-4I(2\rho a)\\
&\quad +[2/(\rho+\mu)a][\mu^2a^2+\rho\mu a^2+(\rho+\mu)a]\\
&\quad +4I(\rho a+\mu a),\\
B_0&=(1/2\rho a)[\mu^2a^2+\rho^2a^2+2\rho a]+2I(2\rho a),
\end{aligned} \quad (3.24)$$

and where

$$I(\gamma a)\equiv e^{\gamma a}\int_1^\infty t^{-2}e^{-\gamma at}dt. \quad (3.25)$$

The procedure we adopt is to minimize H_{tail} with respect to ρ and ϵ while keeping c fixed. This determines values of $\rho=\rho_0$ and $\epsilon=\epsilon_0$. Using the values $\mu a=1$, $3\lambda c^2a^2=24$, and $\beta a^2=56$ from our approximate fit to the spectrum, we obtain $\rho_0 a=2.54$ and $\epsilon_0=0.09$. Using these values of ρ_0 and ϵ_0, we then minimize H with respect to c: $\delta H/\delta c=0=\delta H_{\text{core}}/\delta c+\delta H_{\text{tail}}/\delta c$. At this point it is convenient to introduce the dimensionless parameter α defined as

$$\alpha\equiv G/2(ma)(ca). \quad (3.26)$$

$\delta H/\delta c=0$ then yields the following equation:

$$\begin{aligned}
(3/\pi)\alpha&=[\beta a^2-6-\mu^2a^2-3\lambda c^2a^2]-3[3\lambda c^2a^2A_4\epsilon_0{}^4\\
&\quad +3\lambda c^2a^2A_3\epsilon_0{}^3+(B_2+3\lambda c^2a^2A_2)\epsilon_0{}^2\\
&\quad +(B_1+3\lambda c^2a^2A_1)\epsilon_0+B_0+3\lambda c^2a^2I(4\rho_0 a)].
\end{aligned} \quad (3.27)$$

At this stage all the parameters in the model have been determined with the exception of c, the magnitude of the ground-state pion field. c will be determined by fitting the observed strength of the inelastic form factors. But note that c appears in Eq. (3.27) only in the combination $3\lambda c^2a^2$, and we have already determined an approximate value for this quantity from the fit to the spectrum. Thus Eq. (3.17) and the variational solution for the ground state determine α uniquely. The numerical value obtained is $\alpha=11.1$. One can easily show by looking at $\delta^2H/\delta c^2$ that the variational solution we have obtained indeed corresponds to a minimum in H. We must consider Eq. (3.27) as just a very crude order-of-magnitude estimate of α however, since the right-hand side depends on differences of large numbers which are only poorly determined in this model. The main virtue of our new variational solution is that it gives us a fairly realistic determination of the tail of the pion field, once the value in the source region c is determined.

4. CURRENT OPERATOR

A. Standard Field Theory

In discussing the current operator, we first consider the standard field theory for the pion-nucleon system in which the pion is treated relativistically and the nucleon nonrelativistically. In this standard theory we start from the Hamiltonian

$$H=\frac{1}{2}\int d\mathbf{x}(\dot{\phi}_\alpha\dot{\phi}_\alpha+\nabla\phi_\alpha\cdot\nabla\phi_\alpha+\mu^2\phi_\alpha\phi_\alpha)+\tfrac{1}{4}\lambda\int d\mathbf{x}(\phi_\alpha\phi_\alpha)^2$$
$$-\frac{1}{2}\int d\mathbf{x}\,\beta(x)\phi_\alpha\phi_\alpha+\int d\mathbf{x}\,\psi^\dagger[m+(\mathbf{p}^2/2m)]\psi$$
$$+(G/2m)\int d\mathbf{x}\,\psi^\dagger\tau_\alpha\boldsymbol{\sigma}\cdot\psi\nabla\phi_\alpha. \quad (4.1)$$

We shall neglect the nucleon recoil term $\mathbf{p}^2/2m$. The pion field equation is

$$[\Box-\mu^2-\lambda\phi_\beta\phi_\beta+\beta(x)]\phi_\alpha$$
$$=-(G/2m)\nabla\cdot(\psi^\dagger\tau_\alpha\boldsymbol{\sigma}\psi). \quad (4.2)$$

To generate a conserved current, we make the replacement $\nabla\rightarrow\nabla-ie\mathbf{A}$ in the Hamiltonian (4.1). In the standard theory this is a well-defined procedure, and in particular the result will satisfy gauge invariance. We thus obtain the current

$$\hat{J}_i=-[\boldsymbol{\phi}\times\nabla_i\boldsymbol{\phi}]_3+(G/2m)\psi^\dagger\sigma_i[\boldsymbol{\tau}\times\boldsymbol{\phi}]_3\psi,$$
$$i=1,2,3. \quad (4.3)$$

The first term is the usual Klein-Gordon current. Note that in the present theory the components of the pion field commute:

$$[\phi_\alpha,\phi_\beta]=0. \quad (4.4)$$

Using the field equation (4.2), we compute

$$-\nabla\cdot\hat{\mathbf{J}}\equiv\dot{\hat{\rho}}=[\boldsymbol{\phi}\times\partial^2\boldsymbol{\phi}/\partial t^2]_3$$
$$+(G/2m)\psi^\dagger((\boldsymbol{\sigma}\cdot\nabla)[\boldsymbol{\phi}\times\boldsymbol{\tau}]_3)\psi. \quad (4.5)$$

Again, the first term is the usual Klein-Gordon result.

In our model we make the identification

$$\psi^\dagger\boldsymbol{\sigma}\tau_\alpha\psi\rightarrow S(x)\boldsymbol{\sigma}\tau_\alpha, \quad (4.6)$$

and we then assume the explicit form (3.2) for the nucleon source distribution $S(x)$. The current and time derivative of the charge density arising from the standard field theory are then

$$\hat{J}_i=-[\boldsymbol{\phi}\times\nabla_i\boldsymbol{\phi}]_3^{\rm sym}$$
$$+(G/2m)S(x)\sigma_i[\boldsymbol{\tau}\times\boldsymbol{\phi}]_3^{\rm sym},\quad i=1,2,3$$
$$\dot{\hat{\rho}}=[\boldsymbol{\phi}\times\partial^2\boldsymbol{\phi}/\partial t^2]_3^{\rm sym} \quad (4.7)$$
$$+(G/2m)S(x)(\boldsymbol{\sigma}\cdot\nabla)[\boldsymbol{\phi}\times\boldsymbol{\tau}]_3^{\rm sym};$$

the pion field equation (4.2) becomes

$$[\Box-\mu^2-\lambda\phi_\beta\phi_\beta+\beta\theta(a-x)]\phi_\alpha$$
$$=-(G/2m)\tau_\alpha(\boldsymbol{\sigma}\cdot\nabla)S(x). \quad (4.8)$$

We have chosen to symmetrize $\hat{\mathbf{J}}$ and $\dot{\hat{\rho}}$. Because of Eq. (4.4), this makes no difference in the standard theory. The current is clearly conserved: $\nabla\cdot\hat{\mathbf{J}}+\partial\hat{\rho}/\partial t=0$. (We assume, as in the standard theory, that $[\phi_\beta\phi_\beta,\phi_\alpha]=0$. We will return to this point later.) Knowing $\dot{\hat{\rho}}$, we can compute all the off-diagonal matrix elements of $\hat{\rho}$. We shall show later that for the diagonal matrix elements of ρ we have in addition

$$\langle n|\int\hat{\rho}d\mathbf{x}|n\rangle=\hat{Q}, \quad (4.9)$$

where $\hat{Q}$ is the total charge.

To linearize the theory, we write

$$\phi^\alpha(\mathbf{x},t)=\phi_0{}^\alpha(\mathbf{x})+\eta^\alpha(\mathbf{x},t).$$

Then

$$\hat{J}_i=-[\boldsymbol{\phi}_0\times\nabla_i\boldsymbol{\phi}_0]_3^{\rm sym}+(G/2m)S(x)\sigma_i[\boldsymbol{\tau}\times\boldsymbol{\phi}_0]_3^{\rm sym}$$
$$-[\boldsymbol{\phi}_0\times\nabla_i\boldsymbol{\eta}]_3-[\boldsymbol{\eta}\times\nabla_i\boldsymbol{\phi}_0]_3$$
$$+(G/2m)S(x)\sigma_i[\boldsymbol{\tau}\times\boldsymbol{\eta}]_3,\quad i=1,2,3 \quad (4.10)$$
$$\dot{\hat{\rho}}=[\boldsymbol{\phi}_0\times\partial^2\boldsymbol{\eta}/\partial t^2]_3+(G/2m)S(x)(\boldsymbol{\sigma}\cdot\nabla)[\boldsymbol{\phi}_0\times\boldsymbol{\tau}]_3^{\rm sym}$$
$$+(G/2m)S(x)(\boldsymbol{\sigma}\cdot\nabla)[\boldsymbol{\eta}\times\boldsymbol{\tau}]_3,$$

where we have kept terms to first order in η.

B. Fixed-Source Model

In the fixed-source theory $S(x)$ is taken seriously from the beginning. Capps and Holladay[18] have considered the problem of electromagnetic currents in a fixed-source theory. They show that the substitution $\nabla\rightarrow\nabla-ie\mathbf{A}$ is no longer sufficient to guarantee gauge invariance. To obtain gauge invariance, it is necessary to introduce model-dependent line currents.

To investigate the fixed-source problem in the present treatment without the added complications involved in linearization, we replace the $\lambda\phi^4$ term in the Hamiltonian (3.1) by the following expression:

$$\tfrac{1}{2}\lambda\int d\mathbf{x}(\phi_0{}^\alpha\phi_0{}^\alpha)\phi^\alpha\phi^\alpha. \quad (4.11)$$

In Sec. 4 C we consider the additional problems arising from linearizing the ϕ^4 theory. The corresponding equation of motion is

$$[\Box-\mu^2+\beta\theta(a-x)-\lambda\phi_0{}^\beta\phi_0{}^\beta]\phi^\alpha$$
$$=-(G/2m)\tau^\alpha(\boldsymbol{\sigma}\cdot\nabla)S(x). \quad (4.12)$$

For the ground-state (time-independent) field $\varphi_0{}^\alpha$ the equation is

$$[\nabla^2-\mu^2+\beta\theta(a-x)-\lambda\phi_0{}^\beta\phi_0{}^\beta]\varphi_0{}^\alpha$$
$$=-(G/2m)\tau^\alpha(\boldsymbol{\sigma}\cdot\nabla)S(x). \quad (4.13)$$

By comparing with Eq. (3.4), we see that the potential has been chosen so that $\varphi_0{}^\alpha\equiv\phi_0{}^\alpha$ is a solution. For $\varphi_0{}^\alpha$

[18] R. H. Capps and W. G. Holladay, Phys. Rev. **99**, 931 (1955).

we thus use the variational form given in Eq. (3.9). We then have the result

$$[\tau\times\varphi_0]^{\rm sym}=0=[\tau\times\nabla_i\varphi_0]^{\rm sym}. \tag{4.14}$$

To find the excitations of the system, we again expand about the ground state:

$$\phi^\alpha(\mathbf{x},t)=\varphi_0{}^\alpha(\mathbf{x})+\eta^\alpha(\mathbf{x},t). \tag{4.15}$$

η^α then satisfies the equation

$$[\Box-\mu^2+\beta\theta(a-x)-\lambda\phi_0{}^\beta\phi_0{}^\beta]\eta^\alpha=0. \tag{4.16}$$

The current must contain model-dependent source terms. Therefore, we *choose* the source term so as to produce a conserved current; as a consequence, the lowest order S matrix will be gauge invariant since

$$S^{(1)}=+i\int \hat{J}_\mu A_\mu{}^{\rm ext}d^4x \tag{4.17}$$

is unchanged under the substitution $A_\mu{}^{\rm ext}\to A_\mu{}^{\rm ext}+\partial\Lambda/\partial x_\mu$ if the current is conserved. This follows from a partial integration. We thus *define* the current as follows:

$$\hat{J}_i\equiv-[\phi\times\nabla_i\phi]_3{}^{\rm sym}+(G/2m)S(x)\sigma_i[\tau\times\phi]_3{}^{\rm sym},\quad i=1,2,3. \tag{4.18}$$

To first order in η we have

$$\hat{J}_i=-[\varphi_0\times\nabla_i\varphi_0]_3{}^{\rm sym}-[\varphi_0\times\nabla_i\eta]_3-[\eta\times\nabla_i\varphi_0]_3+(G/2m)S(x)\sigma_i[\tau\times\eta]_3,\quad i=1,2,3. \tag{4.19}$$

Using the field equations, we compute

$$-\nabla\cdot\hat{\mathbf{J}}\equiv\dot{\hat{\rho}}=[\varphi_0\times\partial^2\eta/\partial t^2]_3+(G/2m)S(x)(\boldsymbol{\sigma}\cdot\nabla)[\eta\times\tau]_3. \tag{4.20}$$

The continuity equation is thus satisfied. Let us define the field $\bar{\eta}_\alpha$ by the following:

$$\bar{\eta}_\alpha\equiv i\sum_{nlm}\frac{1}{(2\omega_{nl}{}^3)^{1/2}}[c_{nlm}{}^\alpha\eta_{nlm}(\mathbf{x})e^{-i\omega_{nl}t}-c_{nlm}{}^{\alpha\dagger}\eta_{nlm}{}^\dagger(\mathbf{x})e^{i\omega_{nl}t}]. \tag{4.21}$$

By comparing with Eq. (3.7), we see that

$$\partial\bar{\eta}_\alpha/\partial t=\eta_\alpha. \tag{4.22}$$

The charge density (to second order in η) can thus be written as

$$\hat{\rho}=S(x)\tfrac{1}{2}(1+\tau_3)+[\varphi_0\times\partial\eta/\partial t]_3+[\eta\times\partial\eta/\partial t]_3+(G/2m)S(x)(\boldsymbol{\sigma}\cdot\nabla)[\bar{\eta}\times\tau]_3. \tag{4.23}$$

Using $\partial^2\bar{\eta}^\alpha/\partial t^2=\partial\eta^\alpha/\partial t$ and the field equations for $\varphi_0{}^\alpha$ and η^α, we compute

$$\hat{Q}\equiv\int\hat{\rho}d\mathbf{x}=\tfrac{1}{2}+\tfrac{1}{2}\tau_3+\int d\mathbf{x}[\eta\times\partial\eta/\partial t]_3=\tfrac{1}{2}+\hat{T}_3,\qquad \dot{Q}=i[\hat{H},\hat{Q}]=\int\dot{\rho}d\mathbf{x}=-\int\nabla\cdot\hat{\mathbf{J}}d\mathbf{x}=0. \tag{4.24}$$

Thus, the total charge $\hat{Q}$ computed from $\hat{\rho}$ is a constant and is given by $\frac{1}{2}+\hat{T}_3$. Our definition of the current is therefore satisfactory from this standpoint.

The current $\hat{\mathbf{J}}$ and charge density $\hat{\rho}$ that we have constructed in this modified fixed-source model by requiring current conservation are the same (to first order in η) as the $\hat{\mathbf{J}}$ and $\hat{\rho}$ computed from the standard field theory considered in Sec. 4 A. [Recall that $\varphi_0{}^\alpha\equiv\phi_0{}^\alpha$ and the result (4.14).]

C. Linearization of ϕ^4 Model

We now consider the additional difficulties encountered in constructing the current after linearizing a Hamiltonian such as (3.1) that contains a ϕ^4 meson-meson interaction. One approach is to proceed as in Sec. 4 B, namely, we determine the model-dependent source terms by requiring current conservation. We again define

$$\hat{J}_i\equiv-[\phi\times\nabla_i\phi]_3{}^{\rm sym}+(G/2m)S(x)\sigma_i[\tau\times\phi]_3{}^{\rm sym},\quad i=1,2,3. \tag{4.25}$$

Now, using the field equations (3.4) and (3.6), we compute (to first order in η)

$$-\nabla\cdot\hat{\mathbf{J}}\equiv\dot{\hat{\rho}}=[\phi_0\times\partial^2\eta/\partial t^2]_3+(G/2m)S(x)(\boldsymbol{\sigma}\cdot\nabla)\times[\eta\times\tau]_3+2\lambda(\phi_0)^3(\boldsymbol{\sigma}\cdot\hat{x})[\tau\times\eta]_3. \tag{4.26}$$

The ϕ^4 interaction thus leads to a $\phi_0{}^3$ term in $\dot{\rho}$. The resulting charge density (to second order in η) is

$$\hat{\rho}=S(x)\tfrac{1}{2}(1+\tau_3)+[\phi_0\times\partial\eta/\partial t]_3+[\eta\times\partial\eta/\partial t]_3+(G/2m)S(x)(\boldsymbol{\sigma}\cdot\nabla)[\bar{\eta}\times\tau]_3+2\lambda(\phi_0)^3(\boldsymbol{\sigma}\cdot\hat{x})[\tau\times\bar{\eta}]_3. \tag{4.27}$$

Again, we have the desired properties that

$$\hat{Q}\equiv\int\hat{\rho}d\mathbf{x}=\tfrac{1}{2}+\hat{T}_3,\qquad \dot{Q}=i[\hat{H},\hat{Q}]=0. \tag{4.28}$$

The current $\hat{\mathbf{J}}$ is the same as before, but now the charge density $\hat{\rho}$ contains the extra term

$$2\lambda(\phi_0)^3(\boldsymbol{\sigma}\cdot\hat{x})[\tau\times\bar{\ }]_3.$$

A second approach to linearizing the theory is to take $\hat{J}_\mu$ as an approximation to the current operator in the standard field theory, discussed in Sec. 4 A, to be used in computing the independent matrix elements of $\hat{T}_{LM}{}^{\rm mag}$, $\hat{T}_{LM}{}^{\rm el}$, and $\hat{M}_{LM}{}^{\rm Coul}$, again with the long-wavelength restriction [Eq. (1.5)] built in at the start. In this approach one has

$$\hat{\rho}=S(x)\tfrac{1}{2}(1+\tau_3)+[\phi_0\times\partial\eta/\partial t]_3+(G/2m)S(x)(\boldsymbol{\sigma}\cdot\nabla)[\bar{\eta}\times\tau]_3+[\eta\times\partial\eta/\partial t]_3. \tag{4.29}$$

In both approaches the current is given by

$$\hat{J}_i = -[\phi_0 \times \nabla_i \phi_0]_3^{\text{sym}} - [\phi_0 \times \nabla_i \eta]_3 - [\eta \times \nabla_i \phi_0]_3 + (G/2m) S(x) \sigma_i [\tau \times \eta]_3, \quad i = 1, 2, 3. \quad (4.30)$$

We have performed calculations using both approaches and shall discuss the results in Sec. 6.

Throughout this section we have maintained the assumption that $\dot{\sigma}_\alpha = 0 = \dot{\tau}_\alpha$, and we have been able to develop a *consistent* model in the sense that the model does possess a conserved current. In Appendix B we show that the present model can be considered as the limiting case of a presumably more correct set of equations of motion which permits σ_α and τ_α to have time dependence.

5. COMPUTATION OF MATRIX ELEMENTS

We are now ready to compute the transition matrix elements of the charge and current operators. First, we must construct the states of the theory. It is convenient to employ spherical tensor notation[15] and to introduce spherical creation and destruction operators satisfying the commutation relations

$$[c_{nlm,q}, c_{n'l'm',q'}^\dagger] = \delta_{nn'} \delta_{ll'} \delta_{mm'} \delta_{qq'}. \quad (5.1)$$

The ground state is

$$|G\rangle = |0\rangle \xi_{m_s} \zeta_{m_t}, \quad (5.2)$$

where ξ_{m_s} and ζ_{m_t} are two-component spin and isospin Pauli spinors for the nucleon core and $|0\rangle$ is the vacuum for the meson-field excitations

$$c_{nlm,q}|0\rangle = 0. \quad (5.3)$$

The ground state is just the nucleon with its surrounding static meson field. For an excited state of the nucleon which can be reached through an allowed electromagnetic transition, we write

$$|n(l\tfrac{1}{2}) J M_J T M_T\rangle = \sum_{qq'} \sum_{mm'} (1 q \tfrac{1}{2} q' | 1\tfrac{1}{2} T M_T) \times (l m \tfrac{1}{2} m' | l\tfrac{1}{2} J M_J) c_{nlm,q}^\dagger |0\rangle \xi_{m'} \zeta_{q'}. \quad (5.4)$$

We have coupled the orbital angular momentum of the meson field to the spin $\frac{1}{2}$ of the nucleon core to give a state of definite J, and the isospin 1 of the meson field to the isospin $\frac{1}{2}$ of the core to give a state of definite T. Thus, the excitations have isotopic spin

$$T = \tfrac{1}{2}, \tfrac{3}{2}.$$

The parity of these states can be easily determined. Since the pion field is pseudoscalar, the parity operator in the space of creation and destruction operators for the normal-mode excitations is given by

$$\hat{\Pi} c_{nlm}^{\alpha\dagger} \hat{\Pi}^{-1} = (-1)^{l+1} c_{nlm}^{\alpha\dagger}. \quad (5.5)$$

Thus the parity of the excited states is

$$\hat{\Pi} c_{nlm}^{\alpha\dagger} |0\rangle = (-1)^{l+1} c_{nlm}^{\alpha\dagger} |0\rangle \quad (5.6)$$

or

$$\Pi = (-1)^{l+1} \quad \text{(parity of excitations)}. \quad (5.7)$$

We have used $\hat{\Pi}|0\rangle = |0\rangle$ which follows from the positive parity of the nucleon.

We consider the charge density operator as given in Eq. (4.29):

$$\hat{\rho}(\mathbf{x},t) = S(x)\tfrac{1}{2}(1+\tau_3) + [\phi_0 \times \partial\eta/\partial t]_3 + (G/2m) S(x) (\sigma \cdot \nabla) [\bar{\eta} \times \tau]_3. \quad (5.8)$$

The term $S(x)\frac{1}{2}(1+\tau_3)$ cannot contribute to the transition matrix elements, and so we neglect it for the present. Inserting $\phi_0{}^\alpha = \tau^\alpha (\sigma \cdot \hat{x}) \phi_0$ and the expansions for η^α and $\bar{\eta}^\alpha$, and using spherical tensor notation[15]

$$[\mathbf{a} \times \mathbf{b}]_3 = -\sqrt{2} i \sum_{qq'} (1 q 1 q' | 1110) a_{1q} b_{1q'}, \quad (5.9)$$

where a and b are tensor operators, we find

$$\hat{\rho}(\mathbf{x},t) = \sqrt{2} \sum_{qq'} \sum_{nlm} (1 q 1 q' | 1110) \tau_{1q} [(\tfrac{1}{2}\omega_{nl})^{1/2} (\sigma \cdot \hat{x}) \phi_0(x) + (1/2\omega_{nl}{}^3)^{1/2} (G/2m) S(x) (\sigma \cdot \nabla)] \times [c_{nlm,q'}{}^\dagger \eta_{nlm}{}^\dagger(\mathbf{x}) e^{i\omega_{nl} t} - (-1)^{q'} c_{nlm,-q'} \eta_{nlm}(\mathbf{x}) e^{-i\omega_{nl} t}]. \quad (5.10)$$

The transition matrix elements of the charge density operator are thus

$$\langle n(l\tfrac{1}{2}) J M_J T M_T | \hat{\rho}(\mathbf{x}) | \tfrac{1}{2} m_s, \tfrac{1}{2} m_t \rangle = \sum_{qq'q''} \sum_{mm'} \sqrt{2} [\zeta_{q'}{}^\dagger \tau_{1q''} \zeta_{m_t}] (1 q \tfrac{1}{2} q' | 1\tfrac{1}{2} T M_T) (l m \tfrac{1}{2} m' | l\tfrac{1}{2} J M_J) (1 q'' 1 q | 1110) \times \{ (\tfrac{1}{2}\omega_{nl})^{1/2} \phi_0(x) [\xi_{m'}{}^\dagger (\sigma \cdot \hat{x}) \xi_{m_s}] + (1/2\omega_{nl}{}^3)^{1/2} (G/2m) S(x) [\xi_{m'}{}^\dagger (\sigma \cdot \nabla) \xi_{m_s}] \} R_{nl}{}^\dagger(x) Y_{lm}{}^\dagger(\Omega_x), \quad (5.11)$$

where we have written

$$\eta_{nlm}(\mathbf{x}) = R_{nl}(x) Y_{lm}(\Omega_x). \quad (5.12)$$

The following results are readily established:

$$\begin{aligned} \zeta_{q'}{}^\dagger \tau_{1q''} \zeta_{m_t} &= \sqrt{3} (\tfrac{1}{2} m_t 1 q'' | \tfrac{1}{2} 1 \tfrac{1}{2} q'), \\ \xi_{m'}{}^\dagger (\sigma \cdot \hat{x}) \xi_{m_s} &= -(4\pi)^{1/2} \sum_{m''} (1 m'' \tfrac{1}{2} m' | 1 \tfrac{1}{2} \tfrac{1}{2} m_s) Y_{1m''}(\Omega_x), \\ \xi_{m'}{}^\dagger (\sigma \cdot \nabla) \xi_{m_s} &= -\sqrt{3} \sum_{m''} (1 m'' \tfrac{1}{2} m' | 1 \tfrac{1}{2} \tfrac{1}{2} m_s) \nabla_{m''}. \end{aligned} \quad (5.13)$$

We project out the LMth multipole as needed in Eq. (2.7) using

$$\int Y_{lm}^*(\Omega_x)Y_{1m''}(\Omega_x)Y_{LM}(\Omega_x)d\Omega_x=(-1)^m\left[\frac{(2L+1)(3)(2l+1)}{4\pi}\right]^{1/2}\begin{pmatrix}L & l & 1\\ 0 & 0 & 0\end{pmatrix}\begin{pmatrix}L & l & 1\\ M & -m & m''\end{pmatrix} \tag{5.14}$$

and

$$\int Y_{LM}(\Omega_x)\nabla_{m''}[Y_{lm}^*(\Omega_x)R_{nl}^\dagger(x)]d\Omega_x=(-1)^m[(2L+1)(2l+1)]^{1/2}\begin{pmatrix}L & l & 1\\ 0 & 0 & 0\end{pmatrix}\begin{pmatrix}L & l & 1\\ M & -m & m''\end{pmatrix}$$
$$\times\begin{cases}\left(\dfrac{d}{dx}-\dfrac{l}{x}\right)R_{nl}^\dagger(x), & L=l+1\\ \left(\dfrac{d}{dx}+\dfrac{l+1}{x}\right)R_{nl}^\dagger(x), & L=l-1.\end{cases} \tag{5.15}$$

From the above we find

$$\langle n(l\tfrac{1}{2})JM_JTM_T|\hat{M}_{LM}^{\text{Coul}}(q^*)|\tfrac{1}{2}+m_s,\tfrac{1}{2}m_t\rangle$$
$$=-\sqrt{6}[(2L+1)(3)(2l+1)]^{1/2}\sum_{mm'm''}\sum_{qq'q''}\begin{pmatrix}L & l & 1\\ 0 & 0 & 0\end{pmatrix}\begin{pmatrix}L & l & 1\\ M & -m & m''\end{pmatrix}(-1)^m(1m''\tfrac{1}{2}m'|1\tfrac{1}{2}\tfrac{1}{2}m_s)(\tfrac{1}{2}m_t1q''|\tfrac{1}{2}1\tfrac{1}{2}q')$$
$$\times(1q\tfrac{1}{2}q'|1\tfrac{1}{2}TM_T)(lm\tfrac{1}{2}m'|l\tfrac{1}{2}JM_J)(1q''1q|1110)\left[\int j_L(q^*x)(\tfrac{1}{2}\omega_{nl})^{1/2}\Phi_{nlL}(x)R_{nl}^\dagger(x)x^2dx\right], \tag{5.16}$$

where

$$\Phi_{nlL}(x)R_{nl}^\dagger(x)=\left[\phi_0(x)+\frac{1}{\omega_{nl}^2}\frac{G}{2m}S(x)\left(\frac{d}{dx}-\frac{l}{x}\right)\right]R_{nl}^\dagger(x), \qquad L=l+1$$
$$=\left[\phi_0(x)+\frac{1}{\omega_{nl}^2}\frac{G}{2m}S(x)\left(\frac{d}{dx}+\frac{l+1}{x}\right)\right]R_{nl}^\dagger(x), \quad L=l-1. \tag{5.17}$$

Using standard angular momentum recoupling techniques,[15] we have

$$\langle n(l\tfrac{1}{2})JM_JTM_T|\hat{M}_{LM}^{\text{Coul}}(q^*)|\tfrac{1}{2}+m_s,\tfrac{1}{2}m_t\rangle$$
$$=-\left[\int j_L(q^*x)(\tfrac{1}{2}\omega_{nl})^{1/2}\Phi_{nlL}(x)R_{nl}^\dagger(x)x^2dx\right][(2L+1)(3)(2l+1)]^{1/2}\begin{pmatrix}L & l & 1\\ 0 & 0 & 0\end{pmatrix}(2J+1)^{1/2}\begin{Bmatrix}\frac{1}{2} & 1 & \frac{1}{2}\\ l & J & L\end{Bmatrix}(-1)^M$$
$$\times(L-MJM_J|LJ\tfrac{1}{2}m_s)3[2(2T+1)]^{1/2}\begin{Bmatrix}\frac{1}{2} & 1 & \frac{1}{2}\\ 1 & T & 1\end{Bmatrix}(10TM_T|1T\tfrac{1}{2}M_T). \tag{5.18}$$

Reading off the reduced matrix element, we have finally,

$$\tfrac{1}{2}(4\pi)|\langle n(l\tfrac{1}{2})JTM_T\|\hat{M}_L^{\text{Coul}}(q^*)\|\tfrac{1}{2}+\tfrac{1}{2}m_t\rangle|^2$$
$$=27(4\pi)(2T+1)[(2L+1)(2l+1)(2J+1)]\begin{pmatrix}L & l & 1\\ 0 & 0 & 0\end{pmatrix}^2\begin{Bmatrix}\frac{1}{2} & 1 & \frac{1}{2}\\ l & J & L\end{Bmatrix}^2\begin{Bmatrix}\frac{1}{2} & 1 & \frac{1}{2}\\ 1 & T & 1\end{Bmatrix}^2$$
$$\times(10TM_T|1T\tfrac{1}{2}M_T)^2\omega_{nl}\left|\int j_L(q^*x)\Phi_{nlL}(x)R_{nl}^\dagger(x)x^2dx\right|^2, \tag{5.19}$$

where $\Phi_{nlL}(x)R_{nl}^{\dagger}(x)$ is defined in Eq. (5.17). Observe that all the selection rules are contained in the 3-j and 6-j coefficients

$$\begin{aligned} &\text{(i)} \quad L+l+1 \quad \textit{even} \qquad \text{(parity)} \\ &\qquad L=l\pm 1, \\ &\text{(ii)} \quad L=J\pm\tfrac{1}{2}, \\ &\qquad J=l\pm\tfrac{1}{2}, \\ &\text{(iii)} \quad T=\tfrac{1}{2},\tfrac{3}{2}. \end{aligned} \tag{5.20}$$

If we had started with Eq. (4.27) for $\hat{\rho}$, then the result would have been exactly the same as Eq. (5.19) except that in the definition of $\Phi_{nlL}(x)$ we would have had to make the replacement

$$\phi_0(x) \rightarrow \phi_0(x) - (1/\omega_{nl}^2)2\lambda[\phi_0(x)]^3. \tag{5.21}$$

The LMth electric multipole is given by Eq. (2.14). Keeping only terms linear in η, we have from Eqs. (4.19) and (4.20)

$$\begin{aligned} \nabla\cdot\hat{\mathbf{J}} \equiv -\dot{\rho} &= -\epsilon_{\alpha\beta 3}\tau_\alpha\boldsymbol{\sigma}\cdot\left[\hat{x}\phi_0(x)\frac{\partial^2}{\partial t^2} - \frac{G}{2m}S(x)\nabla\right]\eta_\beta, \\ \mathbf{x}\cdot\hat{\mathbf{J}} &= -\epsilon_{\alpha\beta 3}\tau_\alpha(\boldsymbol{\sigma}\cdot\mathbf{x})[\phi_0(x)\hat{x}\cdot\nabla - (G/2m)S(x)]\eta_\beta. \end{aligned} \tag{5.22}$$

Comparing with Eq. (5.10), we see that

$$\langle f|\nabla\cdot\hat{\mathbf{J}}|i\rangle = -i\omega_{nl}\langle f|\hat{\rho}|i\rangle \tag{5.23}$$

and that $\langle f|\mathbf{x}\cdot\hat{\mathbf{J}}|i\rangle$ can be obtained from the matrix elements of the first term of $\hat{\rho}$ by making the replacement

$$\phi_0(x) \rightarrow \frac{i}{\omega_{nl}}\left[\phi_0(x)x\frac{\partial}{\partial x} - x\frac{G}{2m}S(x)\right]. \tag{5.24}$$

We thus have

$$\begin{aligned} &\langle n(l\tfrac{1}{2})JM_JTM_T|\hat{T}_{LM}^{\text{el}}(q^*)|\tfrac{1}{2}+m_s,\tfrac{1}{2}m_t\rangle \\ &= (-1)^M(\tfrac{1}{2}\omega_{nl})^{1/2}\left[\frac{(2L+1)(3)(2l+1)}{L(L+1)}\right]^{1/2}\begin{pmatrix} L & l & 1 \\ 0 & 0 & 0\end{pmatrix}(2J+1)^{1/2}\begin{Bmatrix} \frac{1}{2} & 1 & \frac{1}{2} \\ l & J & L\end{Bmatrix}\begin{Bmatrix} \frac{1}{2} & 1 & \frac{1}{2} \\ 1 & T & 1\end{Bmatrix} \\ &\times(L-MJM_J|LJ\tfrac{1}{2}m_s)3[2(2T+1)]^{1/2}(10TM_T|1T\tfrac{1}{2}M_T) \\ &\times\left[\frac{\omega_{nl}}{q^*}\int\Phi_{nlL}(x)R_{nl}^{\dagger}(x)x^2\left(1+x\frac{d}{dx}\right)j_L(q^*x)dx + \frac{q^*}{\omega_{nl}}\int j_L(q^*x)x^3\left[\phi_0(x)\frac{d}{dx} - \frac{G}{2m}S(x)\right]R_{nl}^{\dagger}(x)dx\right]. \end{aligned} \tag{5.25}$$

Computing the reduced matrix element, we find

$$\begin{aligned} &\tfrac{1}{2}(4\pi)|\langle n(l\tfrac{1}{2})JTM_T\|\hat{T}_L^{\text{el}}(q^*)\|\tfrac{1}{2}+\tfrac{1}{2}m_t\rangle|^2 \\ &= 27(4\pi)\omega_{nl}(2T+1)(2J+1)\frac{(2L+1)(2l+1)}{L(L+1)}\begin{pmatrix} L & l & 1 \\ 0 & 0 & 0\end{pmatrix}^2\begin{Bmatrix} \frac{1}{2} & 1 & \frac{1}{2} \\ l & J & L\end{Bmatrix}^2\begin{Bmatrix} \frac{1}{2} & 1 & \frac{1}{2} \\ 1 & T & 1\end{Bmatrix}^2(10TM_T|1T\tfrac{1}{2}M_T)^2 \\ &\times\left|\frac{\omega_{nl}}{q^*}\int\Phi_{nlL}(x)R_{nl}^{\dagger}(x)x^2\left(1+x\frac{d}{dx}\right)j_L(q^*x)dx + \frac{q^*}{\omega_{nl}}\int j_L(q^*x)x^3\left[\phi_0(x)\frac{d}{dx} - \frac{G}{2m}S(x)\right]R_{nl}^{\dagger}(x)dx\right|^2. \end{aligned} \tag{5.26}$$

The selection rules are the same as those given in Eq. (5.20). Again, the choice of Eq. (4.27) for $\hat{\rho}$ would require replacement of Eq. (5.21) in the definition of $\Phi_{nlL}(x)$.

Last, we consider the transition matrix elements of the magnetic multipole operator in Eq. (2.12). Keeping only terms linear in η, we compute from Eq. (4.19)

$$\mathbf{x}\cdot(\nabla\times\hat{\mathbf{J}}) \equiv -\nabla\cdot(\mathbf{x}\times\hat{\mathbf{J}}) = i\epsilon_{\alpha\beta 3}\tau_\alpha\left[2\frac{\phi_0(x)}{x} + \frac{G}{2m}S(x)\right](\boldsymbol{\sigma}\cdot\mathbf{l})\eta_\beta, \tag{5.27}$$

where $\mathbf{l}$ is the angular momentum operator

$$\mathbf{l}\equiv(-i)\mathbf{x}\times\boldsymbol{\nabla}. \tag{5.28}$$

Proceeding as in the case of the Coulomb matrix elements and using (5.9), (5.13), and

$$\int Y_{LM}(\Omega_x)[\xi_{m'}{}^{\dagger}(\boldsymbol{\sigma}\cdot\mathbf{l})\xi_{m_s}]Y_{lm}{}^{*}(\Omega_x)d\Omega_x=\delta_{lL}[L(L+1)]^{1/2}\sqrt{3}\sum_{m''}(1m''lm\,|\,1lLM)(\tfrac{1}{2}m_s1m''\,|\,\tfrac{1}{2}1\tfrac{1}{2}m'), \tag{5.29}$$

we find

$$\langle n(l\tfrac{1}{2})JM_JTM_T\,|\,\hat{T}_{LM}{}^{\mathrm{mag}}(q^*)\,|\,\tfrac{1}{2}+m_s,\tfrac{1}{2}m_t\rangle=i\delta_{lL}3\sqrt{2}(2\omega_{nl})^{-1/2}$$

$$\times\left[\int j_L(q^*x)\left\{2\frac{\phi_0(x)}{x}+\frac{G}{2m}S(x)\right\}R_{nl}{}^{\dagger}(x)x^2dx\right]\sum_{qq'q''}\sum_{mm'm''}(lm\tfrac{1}{2}m'\,|\,l\tfrac{1}{2}JM_J)(1m''lm\,|\,1lLM)(\tfrac{1}{2}m_s1m''\,|\,\tfrac{1}{2}1\tfrac{1}{2}m')$$

$$\times(1q\tfrac{1}{2}q'\,|\,1\tfrac{1}{2}TM_T)(1q''1q\,|\,1110)(\tfrac{1}{2}m_t1q''\,|\,\tfrac{1}{2}1\tfrac{1}{2}q'). \tag{5.30}$$

Again using recoupling techniques, we derive

$$\langle n(l\tfrac{1}{2})JM_JTM_T\,|\,\hat{T}_{LM}{}^{\mathrm{mag}}(q^*)\,|\,\tfrac{1}{2}+m_s,\tfrac{1}{2}m_t\rangle$$

$$=i(-1)^{L+M-1}\delta_{lL}\frac{3}{(\omega_{nl})^{1/2}}\sqrt{3}[(2J+1)(2L+1)(2T+1)]^{1/2}\begin{Bmatrix}\frac{1}{2} & 1 & \frac{1}{2}\\ L & J & L\end{Bmatrix}\begin{Bmatrix}\frac{1}{2} & 1 & \frac{1}{2}\\ 1 & T & 1\end{Bmatrix}(L-MJM_J\,|\,LJ\tfrac{1}{2}m_s)$$

$$\times(10TM_T\,|\,1T\tfrac{1}{2}M_T)\left[\int j_L(q^*x)\left\{2\frac{\phi_0(x)}{x}+\frac{G}{2m}S(x)\right\}x^2R_{nl}{}^{\dagger}(x)dx\right]. \tag{5.31}$$

Calculating the reduced matrix element, we have

$$\tfrac{1}{2}(4\pi)\,|\,\langle n(l\tfrac{1}{2})JTM_T\|\hat{T}_L{}^{\mathrm{mag}}(q^*)\|\tfrac{1}{2}+\tfrac{1}{2}m_t\rangle\,|^2$$

$$=(4\pi/\omega_{nl})108\delta_{lL}(2L+1)(2J+1)(2T+1)\begin{Bmatrix}\frac{1}{2} & 1 & \frac{1}{2}\\ L & J & L\end{Bmatrix}^2\begin{Bmatrix}\frac{1}{2} & 1 & \frac{1}{2}\\ 1 & T & 1\end{Bmatrix}^2(10TM_T\,|\,1T\tfrac{1}{2}M_T)^2$$

$$\times\left|\int R_{nl}{}^{\dagger}(x)j_L(q^*x)\left[\frac{\phi_0(x)}{x}+\frac{G}{4m}S(x)\right]x^2dx\right|^2. \tag{5.32}$$

Note that we now have the selection rule $L=l$ instead of $L=l\pm1$ as for the electric and Coulomb terms. The results (ii) and (iii) of Eq. (5.20) still hold. The result (5.32) is the same regardless of the choice of Eq. (4.29) or Eq. (4.27) for the charge density $\hat{\rho}$. We note that the isospin dependence is contained in a factor

$$\begin{aligned}(2T+1)\begin{Bmatrix}\frac{1}{2} & 1 & \frac{1}{2}\\ 1 & T & 1\end{Bmatrix}^2(10TM_T\,|\,1T\tfrac{1}{2}M_T)^2&=2/27, \quad T=\tfrac{1}{2}\\ &=1/27, \quad T=\tfrac{3}{2}.\end{aligned} \tag{5.33}$$

Therefore, other things being equal, the $T=\frac{1}{2}$ levels will be excited twice as strongly as the $T=\frac{3}{2}$ levels in this model.

In Eq. (3.15) we have given the form for $R_{nl}(x)$ used in our model; the source function $S(x)$ is given in Eq. (3.2). Using these expressions and $\phi_0(x)=c$ in the overlap region, and evaluating the 3-j and 6-j coefficients, we find

$$\tfrac{1}{2}(4\pi)\,|\,\langle J_f\|\hat{M}_L{}^{\mathrm{Coul}}\|J_i\rangle\,|^2=\frac{8\pi(2J+1)}{3(2T+1)}(\mu a)(ca)^2\left(\frac{\omega_{1l}}{\mu}\right)\left[\frac{2}{j_{l+1}{}^2(X_{1l})}\right]$$

$$\times\left|\frac{1}{X_{1l}{}^3}\int_0^{X_{1l}}j_L(q_{1l}t)t^2\left[j_l(t)\pm\alpha X_{1l}\frac{3}{\pi}\frac{1}{(\omega_{1l}a)^2}\left(1-\frac{t}{X_{1l}}\right)j_{l\mp1}(t)\right]dt\right|^2 \quad (\text{if } L=l\mp1), \tag{5.34}$$

$$\tfrac{1}{2}(4\pi)\,|\,\langle J_f\|\hat{T}_L{}^{\mathrm{mag}}\|J_i\rangle\,|^2=\frac{32\pi\delta_{lL}}{3(2T+1)}(2J+1)(\mu a)(ca)^2P_{Jl}(L)\left[\frac{2}{j_{l+1}{}^2(X_{1l})}\right]\frac{1}{(\omega_{1l}a)(\mu a)}$$

$$\times\left|\frac{1}{X_{1l}{}^3}\int_0^{X_{1l}}j_L(q_{1l}t)j_l(t)t^2\left[\frac{X_{1l}}{t}+\frac{\alpha}{2}\frac{3}{\pi}\left(1-\frac{t}{X_{1l}}\right)\right]dt\right|^2, \tag{5.35}$$

where

$$P_{Jl}(L)=L/(L+1), \quad J=l+\tfrac{1}{2}$$
$$=(L+1)/L, \quad J=l-\tfrac{1}{2}, \tag{5.36}$$

and

$$\tfrac{1}{2}(4\pi)|\langle J_f\|\hat{T}_L{}^{\mathrm{el}}\|J_i\rangle|^2$$
$$=\frac{8\pi}{3(2T+1)}\frac{2J+1}{L(L+1)}(\mu a)(ca)^2\left(\frac{\omega_{1l}}{\mu}\right)\left[\frac{2}{j_{l+1}{}^2(X_{1l})}\right]\left|\frac{1}{X_{1l}{}^3}\frac{\omega_{1l}}{q^*}\int_0^{X_{1l}}t^2\left[j_l(t)\pm\alpha X_{1l}\frac{3}{\pi}\frac{1}{(\omega_{1l}a)^2}\left(1-\frac{t}{X_{1l}}\right)j_{l\mp1}(t)\right]\right.$$
$$\times[(L+1)j_L(q_{1l}t)-q_{1l}tj_{L+1}(q_{1l}t)]dt+\frac{1}{X_{1l}{}^3}\frac{q^*}{\omega_{1l}}\int_0^{X_{1l}}t^2j_L(q_{1l}t)$$
$$\left.\times\left[\left\{l-\frac{t}{X_{1l}}\frac{3}{\pi}\alpha\left(1-\frac{t}{X_{1l}}\right)\right\}j_l(t)-tj_{l+1}(t)\right]dt\right|^2 \quad (\text{if } L=l\mp1). \tag{5.37}$$

Wherever a $\pm$ or $\mp$ appears, the upper sign applies for the case $L=l-1$ ($J=l-\frac{1}{2}$, normal parity) and the lower sign applies for the case $L=l+1$ ($J=l+\frac{1}{2}$, abnormal parity). We have written the integrals in terms of dimensionless variables and have defined

$$q_{1l}\equiv q^*a/X_{1l}. \tag{5.38}$$

Recall that X_{1l} is the first zero of the lth Bessel function. They are given in Table I. The parameter α is defined in Eq. (3.26). We compute ω_{1l} from the experimental masses of the various resonances as follows. We calculate the total energy in the c.m. system

$$W=[\mathbf{k}^2+\mu^2]^{1/2}+[\mathbf{k}^2+m^2]^{1/2}\approx M, \tag{5.39}$$

and identify this with the mass of the resonance. We then obtain

$$\omega_{1l}=(M^2+\mu^2-m^2)/2M. \tag{5.40}$$

These values are given in Table II. If we had started with Eq. (4.27) for $\hat{\rho}$, then we would have obtained the same results except for the replacement

$$j_l(t)\rightarrow j_l(t)[1-2\lambda c^2a^2/(\omega_{1l}a)^2] \tag{5.41}$$

in the first term of the integral in Eq. (5.34) and in the first term of the first integral in Eq. (5.37).

We can also use our model to compute *elastic* scattering and magnetic properties of the ground state of the nucleon. Now

$$\int e^{i\mathbf{q}^*\cdot\mathbf{x}}\langle\tfrac{1}{2}+\tfrac{1}{2}m_t|\hat{\rho}(\mathbf{x})|\tfrac{1}{2}+\tfrac{1}{2}m_t\rangle d\mathbf{x}$$
$$=\zeta_{m_t}{}^\dagger[\tfrac{1}{2}(1+\tau_3)]\zeta_{m_t}\int e^{i\mathbf{q}^*\cdot\mathbf{x}}S(x)d\mathbf{x}, \tag{5.42}$$

and we can therefore identify the isoscalar and isovector elastic charge form factors as

$$G_E{}^S(q^*)=G_E{}^V(q^*)=\int e^{i\mathbf{q}^*\cdot\mathbf{x}}S(x)d\mathbf{x}$$
$$=\frac{12}{q^*a}\left[\frac{2[1-\cos(q^*a)]}{(q^*a)^3}-\frac{\sin(q^*a)}{(q^*a)^2}\right]\underset{q^*a\rightarrow0}{\rightarrow}1$$
$$-(1/15)(q^*a)^2. \tag{5.43}$$

We can thus identify the mean-square charge radius

$$\langle r^2\rangle_E{}^S=\langle r^2\rangle_E{}^V=\tfrac{2}{5}a^2. \tag{5.44}$$

We now consider the current in the ground state. The term $[\boldsymbol{\eta}\times\nabla\boldsymbol{\eta}]_3$ has zero expectation value in the

TABLE I. The quantity X_{1l}.

l	X_{1l}
0	π
1	4.49
2	5.76
3	6.99
4	8.18
5	9.36
6	10.51
7	11.66

TABLE II. The frequency ω_{1l} as calculated from the experimental masses.

State	ω_{1l}/μ
$\frac{3}{2}^+,\frac{3}{2}$ (1236)	1.9
$\frac{1}{2}^+,\frac{1}{2}$ (1400)	2.8
$\frac{3}{2}^-,\frac{1}{2}$ (1512)	3.4
$\frac{5}{2}^-,\frac{1}{2}$ (1670)	4.1
$\frac{5}{2}^+,\frac{1}{2}$ (1688)	4.2
$\frac{7}{2}^+,\frac{3}{2}$ (1920)	5.3
$\frac{7}{2}^-,\frac{1}{2}$ (2190)	6.4
$\frac{11}{2}^+(?),\frac{3}{2}$ (2423)	7.4
$\frac{11}{2}^-(?),\frac{1}{2}$ (2650)	8.3
$\frac{15}{2}^+(?),\frac{3}{2}$ (2850)	9.1

ground state. The only term in Eq. (4.30) with a nonzero expectation value is

$$(\hat{J}_0)_i = -[\phi_0 \times \nabla_i \phi_0]_3^{\text{sym}}, \quad i=1,2,3. \tag{5.45}$$

Using the result

$$\nabla(\sigma\cdot\hat{x}) = \frac{\sigma}{x} - \frac{\hat{x}}{x}(\sigma\cdot\hat{x}) \tag{5.46}$$

and the properties of the Pauli matrices, we find

$$\hat{\mathbf{J}}_0 = 2\tau_3[\sigma\times\mathbf{x}][\phi_0(x)/x]^2. \tag{5.47}$$

We note that $\nabla\cdot\hat{\mathbf{J}}_0=0$, as must be true. The magnetic-dipole form factor is thus given by

$$\mu_z \equiv \frac{\lambda^V \tau_3 \sigma_z}{2m} = \frac{(6\pi)^{1/2}}{iq^*} T_{10}^{\text{mag}}$$

$$= \frac{(6\pi)^{1/2}}{iq^*}\int j_1(q^*x)\mathfrak{Y}_{111}{}^0\cdot[\sigma\times\mathbf{x}]2\tau_3\left[\frac{\phi_0(x)}{x}\right]^2 d\mathbf{x}. \tag{5.48}$$

Therefore,

$$\lambda^V(q^*) = \frac{3m}{q^*}\int j_1(q^*x)x[1-\cos^2\theta]2\left[\frac{\phi_0(x)}{x}\right]^2 d\mathbf{x}$$

$$= \frac{16\pi m}{3}\int\left[\frac{3j_1(q^*x)}{q^*x}\right][x\phi_0(x)]^2 dx. \tag{5.49}$$

In the limit $q^*\to 0$, $\lambda^V(q^*)$ becomes the anomalous isovector magnetic dipole moment of the nucleon.

$$\lambda^V(0) = \tfrac{1}{3}(16\pi m)\int[x\phi_0(x)]^2 dx$$

$$= (8\pi/9)(\mu a)(ca)^2\left(\frac{2m}{\mu}\right)$$

$$\times\left\{1+3\left[\frac{(1-\epsilon_0)^2}{2\rho_0 a}+\frac{2\epsilon_0(1-\epsilon_0)}{(\rho_0+\mu)a}+\frac{\epsilon_0^2}{2\mu a}\right]\right\}. \tag{5.50}$$

ρ_0 and ϵ_0 are the values determined from the variational solution in Sec. 3.

From the expression for $\lambda^V(q^*)$ we have

$$\frac{\lambda^V(q^*)}{\lambda^V(0)} = \frac{\int[3j_1(q^*x)/q^*x][\phi_0(x)]^2 d\mathbf{x}}{\int[\phi_0(x)]^2 d\mathbf{x}} \xrightarrow[q^*\to 0]{} 1$$

$$-\frac{q^{*2}}{10}\frac{\int x^2[\phi_0(x)]^2 d\mathbf{x}}{\int[\phi_0(x)]^2 d\mathbf{x}}. \tag{5.51}$$

It follows that the mean-square magnetic dipole radius is

$$\langle r^2\rangle_M{}^V = \frac{3}{5}\frac{\int x^2[\phi_0(x)]^2 d\mathbf{x}}{\int[\phi_0(x)]^2 d\mathbf{x}}. \tag{5.52}$$

6. PREDICTIONS OF MODEL AND COMPARISON WITH EXPERIMENT

In this section we present the predictions of the model for the electromagnetic properties of the nucleon and compare the results with experiment where possible. Recall that all the parameters of the model with the exception of c have been roughly determined earlier by either the fit to the nucleon spectrum or the ground-state variational solution. Actually, we carried out a limited search for the best fit to the excitation of the $\frac{3}{2}^+,\frac{3}{2}$ (1236) level using the Stanford[3] and CEA[6] data, and to the excitation of the $\frac{3}{2}^-,\frac{1}{2}$ (1512) and $\frac{5}{2}^+,\frac{1}{2}$ (1688) levels using the CEA[6] data. We computed the inelastic form factors for several sets of values of μa and α. We found the best agreement for the values $\mu a=1$ and $\alpha=10$. This value of μa is the same as that obtained from the fit to the spectrum; this value of α is completely consistent with the value $\alpha=11$ determined from the variational solution. (The results vary slowly with moderate changes of α.) Although the *absolute* minimum of our particular H will occur for negative α and consequently somewhat different potential parameters, we shall take these numbers as an approximate self-consistent best fit. Therefore, in the following all results are computed using the values $\mu a=1$ and $\alpha=10$.

In Figs. 6 and 7 we show the results of calculations for the $\frac{5}{2}^+,\frac{1}{2}$ (1688) level using the two possible forms for the charge density $\hat{\rho}$ of Eqs. (4.27) and (4.29). The magnetic form factor is the same for both cases. We see that in the experimentally allowed region ($q_\mu{}^2\geq 0$) the shape and magnitude of the Coulomb and electric

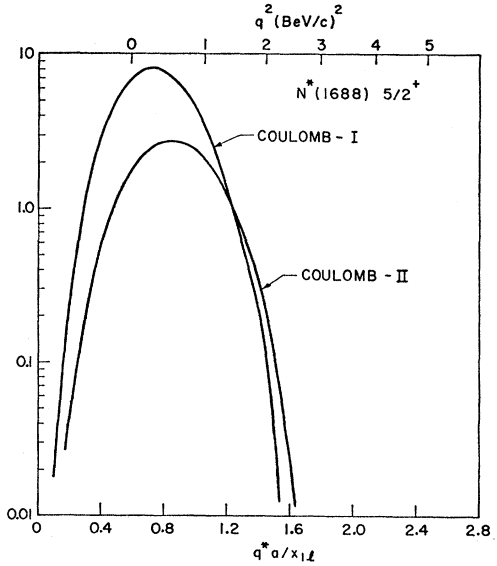

FIG. 6. The reduced Coulomb form factor $|f_c|^2/(\mu a)(ca)^2$ plotted against the reduced momentum transfer $q_{1l}=q^*a/X_{1l}$ for the $\frac{5}{2}^+,\frac{1}{2}$ (1688) level. Curve I is plotted using the charge density $\hat{\rho}$ given in Eq. (4.29); curve II is plotted using the form given in Eq. (4.27).

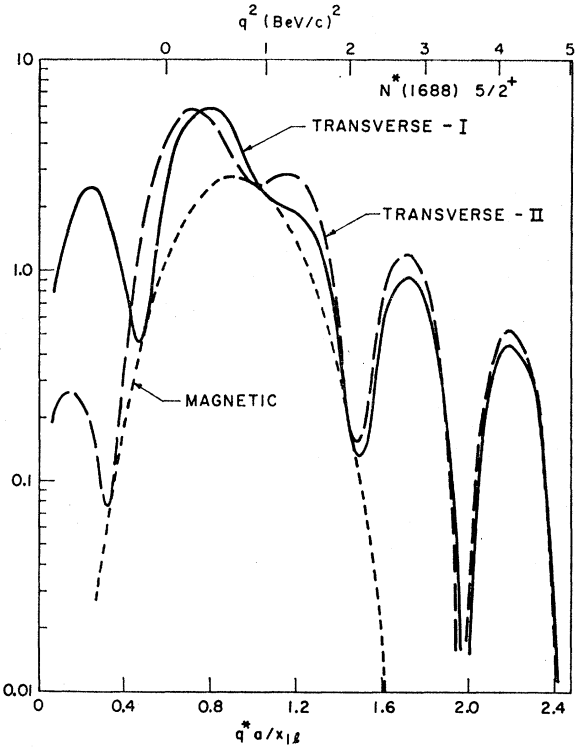

FIG. 7. The reduced transverse form factor $[|f_+|^2+|f_-|^2]/(\mu a)(ca)^2$ plotted against the reduced momentum transfer $q_{1l}=q^*a/X_{1l}$ for the $\frac{5}{2}^+,\frac{1}{2}$ (1688) level. Curve I is obtained using Eq. (4.29) for $\hat{\rho}$; curve II is obtained using Eq. (4.27). The reduced magnetic form factor is also shown. The electric form factor may be found by subtracting the magnetic from the transverse form factor.

form factors do not differ significantly for the two cases. With a few exceptions which we shall discuss later, this conclusion also holds for all the other levels that we have investigated. From the form of Eq. (5.34), which is derived from Eq. (4.29), we see that a cancellation occurs in the Coulomb form factors for the abnormal parity transition. Thus, $|f_c|^2$ should be much larger in the normal than in the abnormal parity transitions, a result that is intuitively appealing. Equation (4.27) leads to the opposite behavior. In addition, the form factors computed from Eq. (4.27) depend explicitly on the value chosen for the coupling constant λ, and this quantity is only very poorly known from our fit to the spectrum. In the authors's opinion, it is preferable to view Eq. (4.29) as an approximation to the true current rather than to introduce another parameter into the current operator itself, and the results we present are obtained using Eq. (4.29) for $\hat{\rho}$.[19] In any event the two approaches give very similar results in the higher resonance region. In Fig. 8 we give $|f_c|^2$ for the normal parity transitions. It is interesting to note that the height of the curves changes by only a factor of three between the lowest and highest resonances shown. Also, the location of the maximum (as a function of q^*a/X_{1l}) increases slightly and the curves become narrower as the energy of the resonance rises. These results are very similar to those of I, although they differ in some details due to the presence of the source term in the charge-density operator in Eq. (4.29).

We expect that our model will be best for the normal parity excitations, which are primarily Coulomb and electric in character. In Fig. 9 we compare the model with the CEA data[6] for the $\frac{3}{2}^-,\frac{1}{2}$ (1512) level. Since these authors do not separate the Coulomb and transverse contributions experimentally, we plot against the directly measured experimental quantity

$$\left[\frac{q^4}{q^{*4}}|f_c|^2+\left(\frac{q^2}{2q^{*2}}+\frac{M^2}{m^2}\tan^2(\tfrac{1}{2}\theta)\right)[|f_+|^2+|f_-|^2]\right]_{\theta=31^\circ}.$$

Note that at photoabsorption, $q^2=0$, and only the last term contributes. We have included the contribution of all the other states which are also supposed to resonate in the indicated region. These states are indicated in

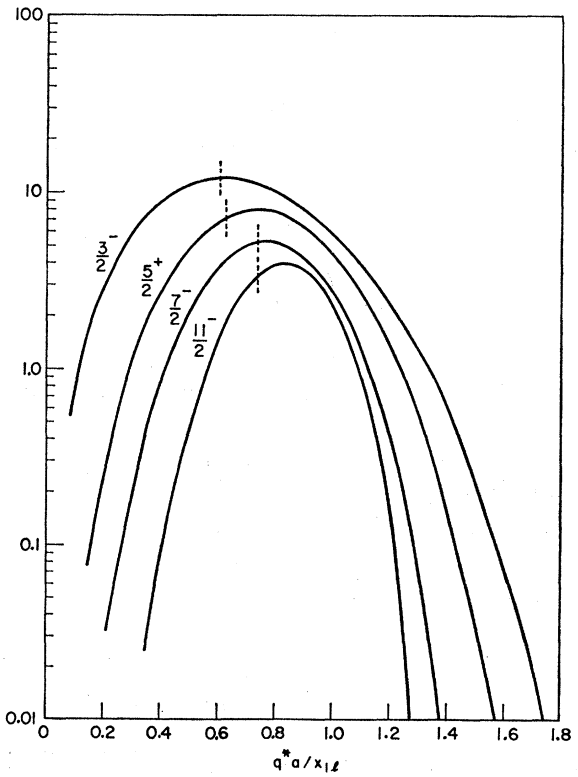

FIG. 8. The reduced Coulomb form factor $|f_c|^2/(\mu a)(ca)^2$ for the normal parity transitions to the levels $\frac{3}{2}^-,\frac{1}{2}$ (1512), $\frac{5}{2}^+,\frac{1}{2}$ (1688), $\frac{7}{2}^-,\frac{1}{2}$ (2190), and $\frac{11}{2}^-$(?),$\frac{1}{2}$ (2650). The threshold $q^2=0$ is indicated for each level by a vertical line.

[19] We have made no attempt to derive a best value of λ from an over-all fit to all the electron scattering data, which is presumably what one should do if Eq. (4.27) is used.

Fig. 9. We see that the over-all shape of the form factor is given quite well and that the dominant contribution comes from the $\frac{3}{2}^-$ level. In Fig. 10 we show the individual form factors for the $\frac{3}{2}^-$ level. We see that at large values of q^2 the $E1$ form factor is completely dominant. This dominance of the electric form factor at large momentum transfers is predicted by the model for all levels, abnormal as well as normal parity transitions. From the observed transition strength to the $\frac{3}{2}^-$ level we determine the value of c to be $(\mu a)(ca)^2=0.010$. Using this *same* value of c, we then predict the form factor for the next level as shown in Fig. 11. The shape is even better here since the diffraction minima are filled in by the background states. (These diffraction minima most likely arise from our assumptions of a source with uniform gradient and a square-well Klein-Gordon potential, and they are probably spurious.) The

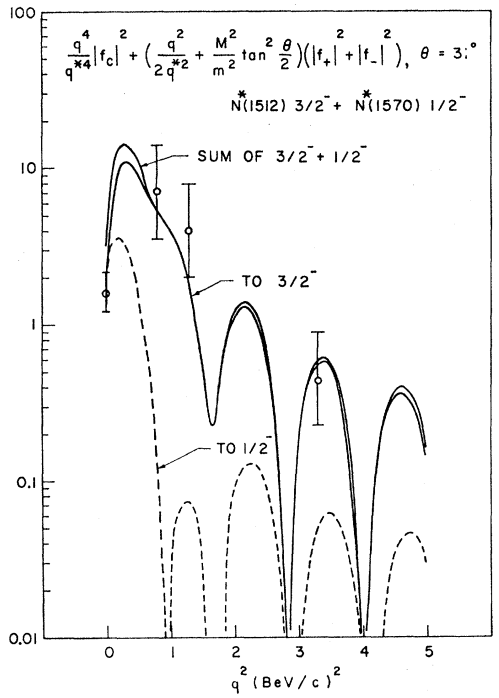

Fig. 9. Reduced inelastic electron scattering transition probability

$$\left[\frac{q^4}{q^{*4}}|f_c|^2+\left(\frac{q^2}{2q^{*2}}+\frac{M^2}{m^2}\tan^2(\tfrac{1}{2}\theta)\right)(|f_+|^2+|f_-|^2)\right]_{31^\circ}\Big/\mu a(ca)^2$$

for the $\frac{3}{2}^-,\frac{1}{2}$ (1512) resonance region as computed in the present model and as measured at CEA (see Ref. 6). The background states which are also thought to resonate in this region have been included. Note the ordinate must still be multiplied by $\mu a(ca)^2=0.010$ to get the experimental form factors. [*Note added in proof.* In determining the experimental values at $q^2=0$, we have used the results of I which relate the integrated resonance photoabsorption cross sections to the peak heights through the assumption of a Breit-Wigner resonance form in the laboratory photon energy. In this calculation the widths Γ given by Cone *et al.* (Ref. 6) were used. If instead we assume a Breit-Wigner shape in the total energy in the isobar rest frame and use the values of Γ given by Rosenfeld *et al.* (Ref. 8), then the $q^2=0$ points are raised: 30% for the 1512 region and 60% for the 1688 region (see Fig. 11).]

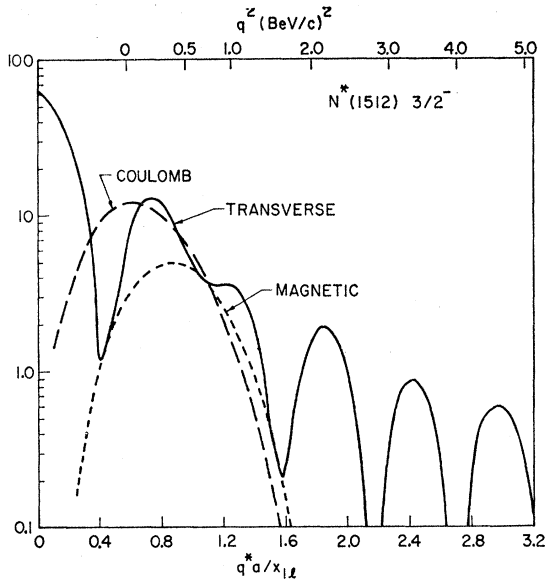

Fig. 10. The reduced Coulomb $|f_c|^2/(\mu a)(ca)^2$ and transverse $[|f_+|^2+|f_-|^2]/(\mu a)(ca)^2$ form factors for the $\frac{3}{2}^-,\frac{1}{2}$ (1512) level. The reduced magnetic form factor is also shown.

$\frac{5}{2}^+$ state provides the dominant contribution to the curve. It is interesting to note how the role played by the various multipoles and states changes as the momentum transfer is increased. The only real method of sorting out these contributions is to do coincidence experiments on the peak at different momentum transfers.

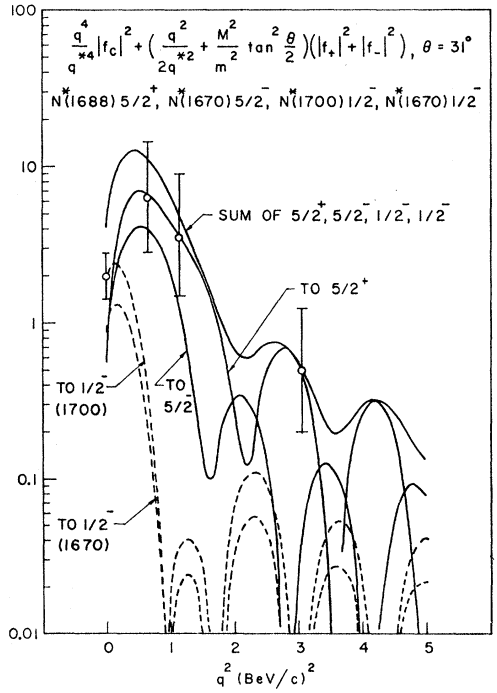

Fig. 11. Same as Fig. 9 for the $\frac{5}{2}^+,\frac{1}{2}$ (1688) resonance region.

For the s-wave background states we have just put our $1S$ state at the observed energies to get the form factors shown and our estimates for these states are therefore very crude. Use of the $2S$ state would give a much smaller contribution to photoproduction without significantly changing the rest of the predicted curve. Figures 6 and 7 present the individual form factors for the $\frac{5}{2}^+$ level, and Fig. 12 gives them for the $\frac{5}{2}^-$ level. The curves calculated using the charge density of Eqs. (4.26) and (4.27) and the standard set of parameters with, again, $\mu a(ca)^2=0.010$, give form factors at 31° essentially indistinguishable from those of Figs. 9 and 11. [*Note added in proof.* The predictions of the model for the cross section at $\theta=47.4°$ are in agreement with our analysis of the DESY data[7] for the 1512 and 1688 resonance regions.]

In the present model the electric transition multipole $\hat{T}_{LM}^{\rm el}$ contains an explicit $\mathbf{x}\cdot\hat{\mathbf{J}}$ term [see Eqs. (2.14) and (5.22)]. Since this term is multiplied by q^{*2}, it does not contribute in the long-wavelength limit $q^*\to 0$, and hence it does not contribute to the relation

$$\frac{|f_+|^2+|f_-|^2}{|f_c|^2}\underset{q^*\to 0}{\approx}\frac{(J+\frac{1}{2})}{(J-\frac{1}{2})}\left(\frac{q_0}{q^*}\right)^2, \tag{6.1}$$

valid for normal parity transitions. The model thus predicts a greater contribution from the transverse form factor at large momentum transfer than one would estimate from Eq. (6.1) alone.[9] The breakdown of the cross section given in I is not grossly in error, according to this model, except at the largest q^2 points where we estimate that the cross section is all transverse.

In Figs. 13–18 we present predictions for the higher

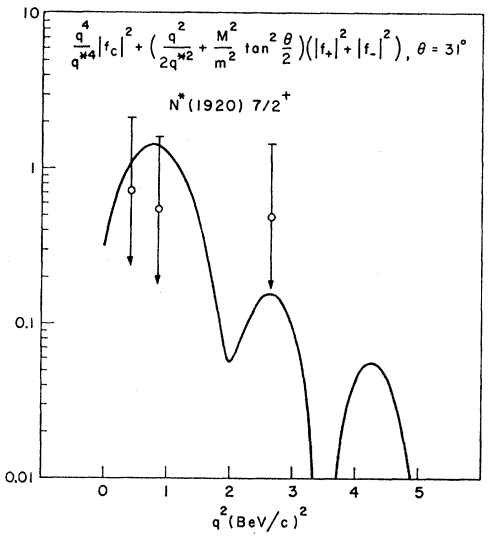

FIG. 13. Same as Fig. 9 for the $\frac{7}{2}^+,\frac{3}{2}$ (1920) resonance state.

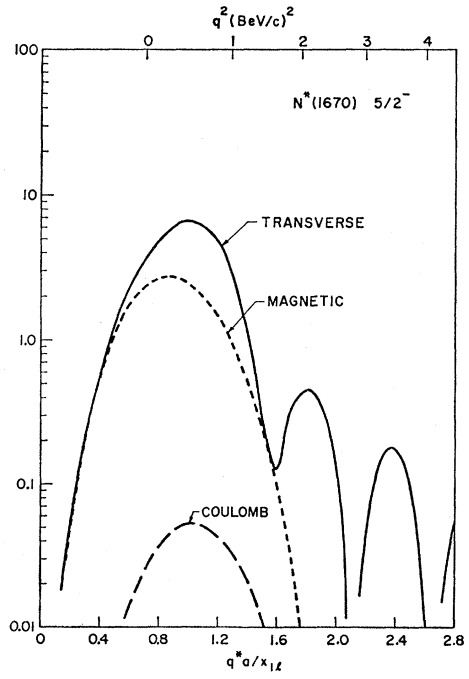

FIG. 12. Same as Fig. 10 for the $\frac{5}{2}^-,\frac{1}{2}$ (1670) level.

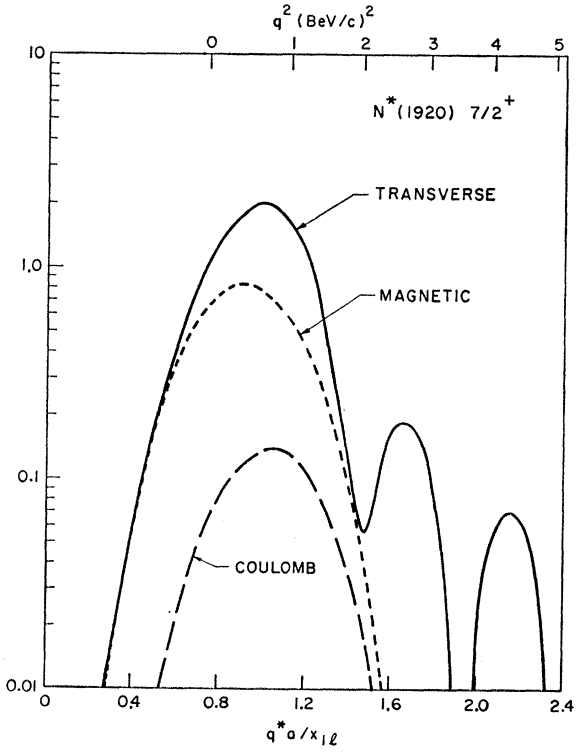

FIG. 14. Same as Fig. 10 for the $\frac{7}{2}^+,\frac{3}{2}$ (1920) level.

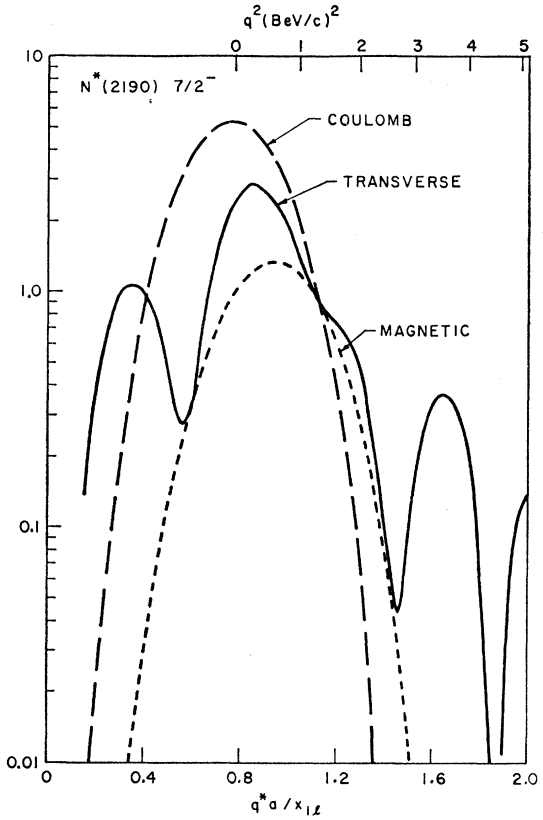

FIG. 15. Same as Fig. 10 for the $\frac{7}{2}^-,\frac{1}{2}$ (2190) level.

resonances. All these curves are computed using the same value of c: $(\mu a)(ca)^2=0.010$.

We expect that the model will be poorest for the

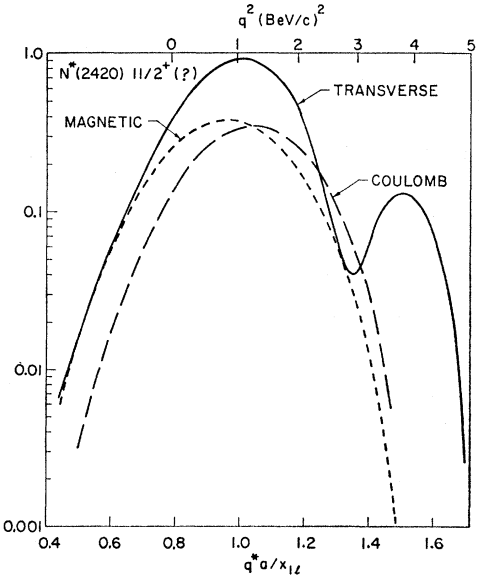

FIG. 16. Same as Fig. 10 for the $\frac{11}{2}^+(?),\frac{3}{2}$ (2420) level.

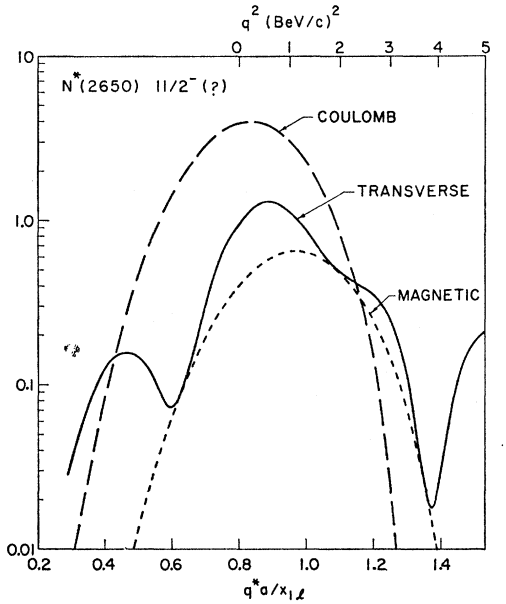

FIG. 17. Same as Fig. 10 for the $\frac{11}{2}^-(?),\frac{1}{2}$ (2650) level.

$\frac{3}{2}^+,\frac{3}{2}$ (1236) level, which is predominantly a magnetic transition and lies lowest in energy. We have however, also carried out a comparison, and the result is shown

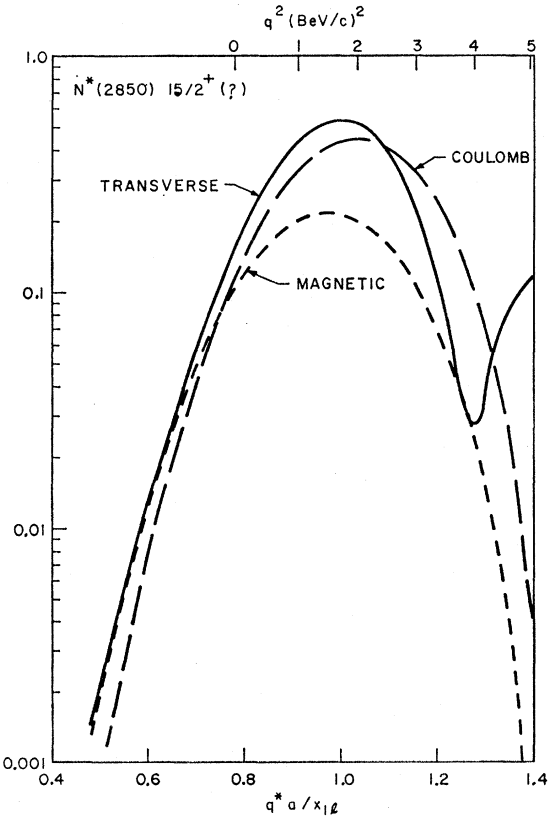

FIG. 18. Same as Fig. 10 for the $\frac{15}{2}^+(?),\frac{3}{2}$ (2850) level.

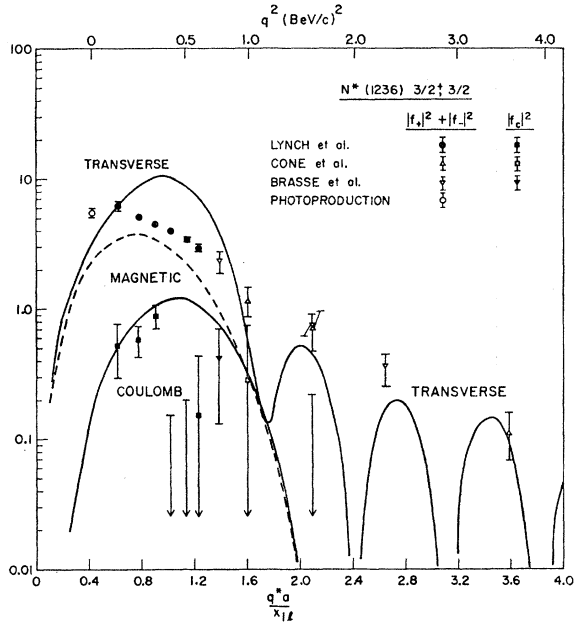

FIG. 19. Same as Fig. 10 for the $\frac{3}{2}^+,\frac{3}{2}$ (1236) level. The experimental data are from Refs. 3, 6, and 7. When only peak heights of the cross section are reported, we assume that the relative background contribution is the same as that of the s wave at photoproduction (25%) and subtract this amount from the peak-height values before determining the integrated resonance cross sections. To get these quantities we then assume a Breit-Wigner resonance shape in the total energy in the isobar rest frame. Note the ordinate must still be multiplied by $\mu a(ca)^2=0.059$ to get the experimental form factors.

in Fig. 19. We need a substantially larger value of c here, $(\mu a)(ca)^2=0.059$.[20] Although the transition is primarily magnetic for small q^2, the model again predicts that at large momentum transfer the electric transition will dominate.

The Roper resonance ($J^\pi=\frac{1}{2}^+$, $T=\frac{1}{2}$, 1400 MeV) can be excited only through Coulomb monopole and magnetic-dipole transitions. In the long-wavelength limit the $C0$ operator is just the total charge,

$$\hat{M}_0{}^{\mathrm{Coul}}(q^*) = \int d\mathbf{x}\, j_0(q^*x)Y_{00}(\Omega_x)\hat{\rho}(\mathbf{x}) \underset{q^*\to 0}{\longrightarrow} \hat{Q}/(4\pi)^{1/2}, \quad (6.2)$$

and this operator cannot cause any transitions. Therefore, $|f_c|^2$ for the Roper resonance must start as q^{*2}. Curve I in Fig. 20 [derived from Eq. (4.29)] clearly violates this requirement; curve II [derived from Eq. (4.27)] at least decreases as $q^*\to 0$, even though it does not actually go to zero. This is the one case where it is necessary to have

$$\int \hat{\rho}\, d\mathbf{x} = \hat{Q} \quad (6.3)$$

hold as an operator identity, not just in diagonal matrix elements. [See Eq. (4.9).] Because of the absence of an electric transition, the predicted cross section for excitation of the Roper resonance falls off rapidly for q^2 greater than 1 (BeV/c)^2.

Taking the limiting case $q_\mu{}^2\to 0$ of our theoretical results, we can compare with the various phenomenological analyses of photoproduction[13,14] that have been carried out in these higher-resonance regions. The relation between the photoproduction amplitudes and the multipole expansion is discussed in Appendix A. The particular result that we need here is Eq. (A11). For all of the levels we have examined, sgn(Integral-mag) $=+$ and sgn(Integral-elec) $=-$ at photoproduction. The sign of the magnetic integral is certainly a general result, and it appears that the sign of the electric integral is also. We thus have

$$\begin{aligned} \frac{E_{l+}}{M_{l+}} &= +\left[\frac{l}{l+2}\right]^{1/2}\left|\frac{\langle J\|\hat{T}_{l+1}{}^{\mathrm{el}}\|\frac{1}{2}\rangle}{\langle J\|\hat{T}_l{}^{\mathrm{mag}}\|\frac{1}{2}\rangle}\right|, \quad J=l+\tfrac{1}{2}; \\ \frac{M_{l-}}{E_{l-}} &= -\left[\frac{l-1}{l+1}\right]^{1/2}\left|\frac{\langle J\|\hat{T}_l{}^{\mathrm{mag}}\|\frac{1}{2}\rangle}{\langle J\|\hat{T}_{l-1}{}^{\mathrm{el}}\|\frac{1}{2}\rangle}\right|, \quad J=l-\tfrac{1}{2}. \end{aligned} \quad (6.4)$$

Table III shows the predictions and the results of the phenomenological analyses. We see that the predicted magnitudes agree quite well with the results of the analyses, but the sign appears to disagree systematically.

TABLE III. Photoproduction amplitudes.

State	Ratio	Walker	Moorhouse *et al.*	Model[a]
$\frac{3}{2}^+,\frac{3}{2}$ (1236)	$E_1{}^+/M_1{}^+$	-0.04 ± 0.08		$+0.34$
$\frac{3}{2}^-,\frac{1}{2}$ (1512)	$M_2{}^-/E_2{}^-$	$+0.53\pm0.2$	$+0.34$	-0.50
$\frac{5}{2}^-,\frac{1}{2}$ (1670)	$E_2{}^+/M_2{}^+$	$-0.5\ \pm0.5$		$+0.52$
$\frac{5}{2}^+,\frac{1}{2}$ (1688)	$M_3{}^-/E_3{}^-$	$+0.5\ \pm0.3$		-0.69
$\frac{7}{2}^+,\frac{3}{2}$ (1920)	$E_3{}^+/M_3{}^+$			$+0.55$
$\frac{7}{2}^-,\frac{1}{2}$ (2190)	$M_4{}^-/E_4{}^-$			-0.64
$\frac{11}{2}^+(?),\frac{3}{2}$ (2423)	$E_5{}^+/M_5{}^+$			$+0.60$
$\frac{11}{2}^-(?),\frac{1}{2}$ (2650)	$M_6{}^-/E_6{}^-$			-0.72
$\frac{15}{2}^+(?),\frac{3}{2}$ (2850)	$E_7{}^+/M_7{}^+$			$+0.60$
Ratios of $\|f_+\|^2+\|f_-\|^2$				
$\frac{1}{2}^-$ (1570)/$\frac{3}{2}^-$ (1512)		0.15 ± 0.2	0.07	1.38
$\frac{5}{2}^-$ (1670)/$\frac{5}{2}^+$ (1688)		0.24 ± 0.3		1.56

[a] These ratios will be modified somewhat if Eq. (4.27) is used for $\hat{\rho}$ instead of Eq. (4.29). The effect is to increase the magnitude of the electric amplitude without changing its sign. The magnetic amplitude is unchanged. The change ranges from about 40% for the lower resonances to about 20% for the higher resonances.

[20] If Eq. (4.27) is used for the charge density, the magnitude of the resulting Coulomb form factor is about ten times greater than that shown in Fig. 19. The ratio of Coulomb to transverse excitation is then inconsistent with the experimental results shown in the figure. The Coulomb form factors for the $\frac{3}{2}^+,\frac{3}{2}$ (1236) and $\frac{1}{2}^+,\frac{1}{2}$ (1400) are the only places where the two different forms of the charge density [Eqs. (4.27) and (4.29)] make any real difference.

When only the final electron is detected, the cross section depends only on the sums of the squares of the amplitudes, and the model's predictions will then agree with experiment. However, the model would give the wrong detailed angular distribution of pions in pion photoproduction. The fact that the s-wave contribution to the integrated photoabsorption cross section is so far off is not surprising since the s waves are treated so very crudely in this model. As noted earlier, use of the $2S$ instead of the $1S$ state would give a negligible contribution to photoproduction. Our model does appear to have too much photoproduction of the $\frac{5}{2}^-$ in the third resonance region, although it does predict that the $\frac{5}{2}^+$ dominates the inelastic form factor.

The model developed in I and the present paper was intended to provide predictions for the excitation of the higher nucleon resonances, and the approximations made were appropriate for this goal. However, the model does permit calculation of ground-state properties of the nucleon, and for completeness we shall include these results. One should not expect close agreement with experiment since in addition to questionable approximations, zero-point quantum fluctuations are quite important in the ground state. This last point is discussed in I. From Eqs. (5.44) and (5.52) we find that the value of the range (a) we use gives the root-mean-square radius for the charge and magnetic moment of the nucleon as measured in elastic scattering to within 10 and 30%, respectively. We find

$$(\langle r^2\rangle_E{}^S)^{1/2}=(\langle r^2\rangle_E{}^V)^{1/2}=0.89\text{ F}$$

and

$$(\langle r^2\rangle_M{}^V)^{1/2}=1.04\text{ F},$$

whereas experimentally

$$(\langle r^2\rangle_E{}^S)^{1/2}\approx(\langle r^2\rangle_E{}^V)^{1/2}=0.8\text{ F}$$

and

$$(\langle r^2\rangle_M{}^V)^{1/2}=0.8\text{ F}.$$

Having determined the value of c by fitting the height of the inelastic excitations, we obtain from Eq. (5.50) the anomalous isovector magnetic moment of the nucleon. The values are shown in Table IV. We have also indicated the value of the pion-nucleon coupling constant derived from Eq. (3.11) using the same parameters. Finally, in Fig. 21 we compare the elastic charge and magnetic-dipole form factors with the best fit to the experimental results. The agreement is not very good, but note that the charge and magnetic-dipole form factors are of about the same magnitude even though they are computed from quite dissimilar expressions.

TABLE IV. The anomalous magnetic moment of the nucleon and the pion-nucleon coupling constant as determined from the fit to the height of the inelastic spectrum.

Resonance region	$(\mu a)(ca)^2$	λ^V	f^2
$\frac{3}{2}^+,\frac{3}{2}$ (1236)	0.059	3.6	0.06
$\frac{3}{2}^-,\frac{1}{2}$ (1512)	0.010	0.62	0.01
$\frac{5}{2}^+,\frac{1}{2}$ (1688)	0.010	0.62	0.01
		$\lambda^V_{\text{exp}}=1.85$	$f^2_{\text{exp}}=0.08$

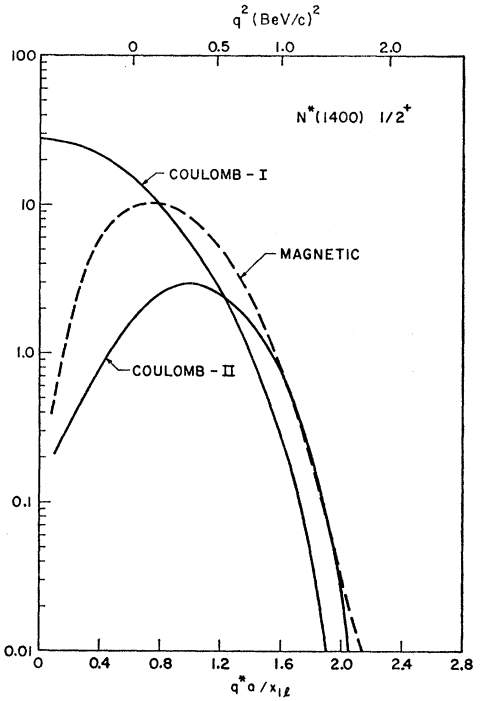

FIG. 20. The reduced Coulomb and magnetic form factors for the Roper resonance. Curve I is obtained from Eq. (4.29); curve II is obtained from Eq. (4.27).

7. CONCLUSIONS

In summary, we have constructed a crude static model of the nucleon which provides a dynamical framework from which one can predict the existence of nucleon resonances. The resulting level spectrum is quite similar to that observed for the nucleon. We have given an improved variational solution for the ground-state pion field and have identified the pion-nucleon coupling constant from the asymptotic form of the field. We have constructed a conserved current and thus can compute all the electromagnetic properties of the nucleon on a consistent basis. In addition, we can investigate the interrelations between these properties. The inelastic form factors agree quite well with the CEA data[6] for the higher resonances and at least semiquantitatively with the data for the 3-3 resonance. The model should be poorest for the 3-3 resonance, and this is indeed the case. One interesting prediction is that the contribution of the various multipole terms changes dramatically as q^2 is varied. The predictions for the ground-state properties should be the least reliable because of the zero-point oscillations of the normal-mode excitations (this is discussed in I), but from fitting the inelastic form factors we do obtain the anomalous isovector magnetic

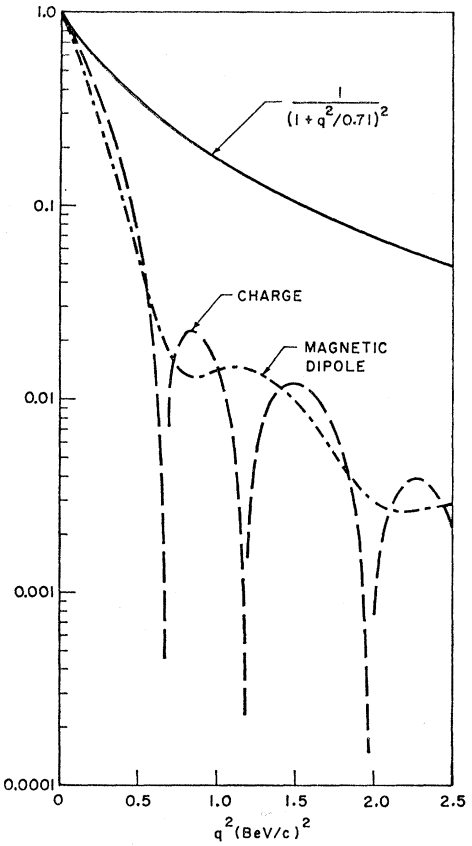

FIG. 21. The magnitude of the elastic charge and anomalous magnetic-dipole form factors as computed in the present model and as given by the dipole fit to experimental data [G. Weber in Proceedings of the 1967 International Symposium on Electron and Photon Interactions at High Energies, Stanford Linear Accelerator Center, Stanford, Calif. (to be published)]:

$$G_{EP}=\frac{G_{MP}}{\mu_p}=\frac{G_{Mn}}{\mu_n}=\frac{1}{[1+q^2/(0.71\ \mathrm{BeV}^2)]^2},\quad G_{En}\approx 0.$$

Note that the anomalous magnetic-moment form factor $[F_2^V(q^2)/F_2^V(0)]$ differs from the total magnetic form factor $[G_M^V(q^2)/G_M^V(0)]$ by a factor $(1+q^2/4m^2)^{-1}$. This term is relatively unimportant over this range of q^2.

moment of the nucleon to within a factor of three and the elastic root-mean-square radius to within 25%. In the limit of photoproduction we get the right ratios for $|M_{l\pm}/E_{l\pm}|^2$, which are the quantities that enter into electron scattering. The sign we get for this ratio, however, appears to systematically disagree with that obtained in the phenomenological analysis of pion photoproduction, and thus a more detailed model is needed to obtain the exact angular distribution in this process.

The model presented is a naive one, and it is in no sense a complete theory of the nucleon. Even within the framework of the model, improvements could be made. Thus one would like to find some mechanism for the generation of the potential scattering term, which is essential to the model, and repeat the calculation with a more realistic potential which should also explain the widths of the resonances and with the vacuum-fluctuation corrections included. Also, one could determine the source density $S(x)$ from elastic scattering. Despite these shortcomings, the model does provide a dynamical framework in which to investigate the electromagnetic properties of the nucleon, and the interrelations between these quantities, on a consistent basis.

ACKNOWLEDGMENT

The authors wish to thank Dr. E. Nyman for a very valuable discussion.

APPENDIX A: RELATION TO PHOTOPRODUCTION AMPLITUDES

In this Appendix we establish the connection between the normal photoproduction amplitudes[13,14] and the multipole expansion used in the present work. We use the notation more commonly employed for photoproduction; that is, we label the incoming virtual photon momentum by k and the final pion momentum by q. Therefore, we have

$$\begin{aligned} k&=p-p',\\ k+P&=P'+q, \end{aligned} \tag{A1}$$

Following Chew, Goldberger, Low, and Nambu,[21] we write the photoproduction amplitude $\mathfrak{F}$ in the isobar rest system for a given isotopic spin configuration as

$$\mathfrak{F}=i\boldsymbol{\sigma}\cdot\boldsymbol{\varepsilon}\mathfrak{F}_1+\frac{(\boldsymbol{\sigma}\cdot\mathbf{q})\boldsymbol{\sigma}\cdot(\mathbf{k}\times\boldsymbol{\varepsilon})}{qk}\mathfrak{F}_2 +i\frac{(\boldsymbol{\sigma}\cdot\mathbf{k})(\mathbf{q}\cdot\boldsymbol{\varepsilon})}{qk}\mathfrak{F}_3+i\frac{(\boldsymbol{\sigma}\cdot\mathbf{q})(\mathbf{q}\cdot\boldsymbol{\epsilon})}{q^2}\mathfrak{F}_4. \tag{A2}$$

$\mathfrak{F}_1\cdots\mathfrak{F}_4$ are functions of energy and angle in the isobar rest system, and $\mathbf{q}$ and $\mathbf{k}$ are the meson and photon three-momenta.

We consider the special case in which the photon is incident with helicity $+1$ and the meson is produced in the forward direction. In order for the amplitude to be nonzero, the baryon spin must flip. In this case $\mathbf{q}\cdot\boldsymbol{\varepsilon}=0$, and the amplitude reduces to

$$\mathfrak{F}_0=\sqrt{2}i[-\mathfrak{F}_1+\mathfrak{F}_2]. \tag{A3}$$

The angular dependence may be made explicit through an expansion involving derivatives of Legendre polynomials[21]:

$$\begin{aligned} \mathfrak{F}_1&=\sum_{l=0}^{\infty}\{[lM_{l+}+E_{l+}]P_{l+1}'(x) +[(l+1)M_{l-}+E_{l-}]P_{l-1}'(x)\},\\ \mathfrak{F}_2&=\sum_{l=1}^{\infty}[(l+1)M_{l+}+lM_{l-}]P_l'(x). \end{aligned} \tag{A4}$$

[21] G. F. Chew, M. L. Goldberger, F. E. Low, and Y. Nambu, Phys. Rev. 106, 1320 (1957).

x is the cosine of the angle of emission in the isobar rest system. The energy-dependent amplitudes $M_{l\pm}$ and $E_{l\pm}$ refer to transitions initiated by magnetic and electric radiation, respectively, leading to final states of orbital angular momentum l and total angular momentum $l\pm\frac{1}{2}$. Each of these amplitudes may be written in terms of three isotopic spin amplitudes. The amplitude $\mathfrak{F}_0$ can thus be written as

$$\mathfrak{F}_0=\sqrt{2}i\{\sum_l [(l+1)M_{l+}P_l'(1)-lM_{l+}P_{l+1}'(1) -E_{l+}P_{l+1}'(1)]+\sum_l [lM_{l-}P_l'(1) -(l+1)M_{l-}P_{l-1}'(1)-E_{l-}P_{l-1}'(1)]\}. \quad \text{(A5)}$$

We now consider this special case of photoproduction from the standpoint of the multipole analysis. The transition operator for photoabsorption is[10]

$$\hat{T}=\int [\mathbf{e}_{k1}\cdot\hat{\mathbf{J}}(\mathbf{x})]e^{i\mathbf{k}\cdot\mathbf{x}}d\mathbf{x} =-(2\pi)^{1/2}\sum_{L=1}^{\infty}(i)^L(2L+1)^{1/2}[\hat{T}_{L1}{}^{\mathrm{el}}+\hat{T}_{L1}{}^{\mathrm{mag}}]. \quad \text{(A6)}$$

Introducing reduced matrix elements, we write

$$\langle J^\pi\tfrac{1}{2}|\hat{T}|\tfrac{1}{2}+-\tfrac{1}{2}\rangle=(2\pi)^{1/2}\sum_{L=1}^{\infty}(i)^L(J^\pi\tfrac{1}{2}\tfrac{1}{2}\tfrac{1}{2}|J^\pi\tfrac{1}{2}L1) \times\langle J^\pi\|(\hat{T}_L{}^{\mathrm{el}}+\hat{T}_L{}^{\mathrm{mag}})\|\tfrac{1}{2}^+\rangle. \quad \text{(A7)}$$

We now consider the excitation of a particular isobar with $J=l\pm\frac{1}{2}$. Employing Eqs. (A5) and (A7) and the result

$$P_l'(1)=\tfrac{1}{2}l(l+1), \quad \text{(A8)}$$

we find

$$\frac{E_{l+}}{M_{l+}}=-i\left[\frac{l}{l+2}\right]^{1/2}\frac{\langle J\|\hat{T}_{l+1}{}^{\mathrm{el}}\|\frac{1}{2}\rangle}{\langle J\|\hat{T}_l{}^{\mathrm{mag}}\|\frac{1}{2}\rangle}, \quad J=l+\tfrac{1}{2};$$
$$\frac{M_{l-}}{E_{l-}}=+i\left[\frac{l-1}{l+1}\right]^{1/2}\frac{\langle J\|\hat{T}_l{}^{\mathrm{mag}}\|\frac{1}{2}\rangle}{\langle J\|\hat{T}_{l-1}{}^{\mathrm{el}}\|\frac{1}{2}\rangle}, \quad J=l-\tfrac{1}{2}. \quad \text{(A9)}$$

The relations (A9) between the two sets of amplitudes are completely general. We next use the reduced matrix elements as calculated in our model to determine the relative phase. From Eqs. (5.25) and (5.31) we find after some algebra the following relative phases:

$$\begin{aligned}&\text{Magnetic:}\quad i\,\mathrm{sgn}(\text{Integral-mag});\\ &\text{Electric:}\quad +\mathrm{sgn}(\text{Integral-elec}),\quad J=l+\tfrac{1}{2}\\ &\qquad\quad -\mathrm{sgn}(\text{Integral-elec}),\quad J=l-\tfrac{1}{2}.\end{aligned} \quad \text{(A10)}$$

sgn(Integral-mag) is the *sign* of the integral appearing in the matrix element of $\hat{T}_L{}^{\mathrm{mag}}$ in Eq. (5.31); sgn(Integral-elec) has a similar meaning for the integral appearing in Eq. (5.25). We thus have the desired relationship between our model and the photoproduction amplitudes:

$$\frac{E_{l+}}{M_{l+}}=-\left[\frac{l}{l+2}\right]^{1/2}\frac{\mathrm{sgn}(\text{Integral-elec})}{\mathrm{sgn}(\text{Integral-mag})}\left|\frac{\langle J\|\hat{T}_{l+1}{}^{\mathrm{el}}\|\frac{1}{2}\rangle}{\langle J\|\hat{T}_l{}^{\mathrm{mag}}\|\frac{1}{2}\rangle}\right|, \quad J=l+\tfrac{1}{2}; \quad \text{(A11)}$$
$$\frac{M_{l-}}{E_{l-}}=+\left[\frac{l-1}{l+1}\right]^{1/2}\frac{\mathrm{sgn}(\text{Integral-mag})}{\mathrm{sgn}(\text{Integral-elec})}\left|\frac{\langle J\|\hat{T}_l{}^{\mathrm{mag}}\|\frac{1}{2}\rangle}{\langle J\|\hat{T}_{l-1}{}^{\mathrm{el}}\|\frac{1}{2}\rangle}\right|, \quad J=l-\tfrac{1}{2}.$$

APPENDIX B: COUPLED EQUATIONS OF MOTION

In this Appendix we derive a set of coupled equations of motion for $\boldsymbol{\phi}$, $\boldsymbol{\sigma}$, and $\boldsymbol{\tau}$ which do not require $\dot{\sigma}_\alpha=0=\dot{\tau}_\alpha$,[16] and thus presumably are more correct than those employed in the model presented in the body of the paper. But we also show that the model presented so far is a limiting case of the (more correct) model to be developed here. For the choice of parameters made in the text the results of the two models should not be significantly different with the possible exception of the 3-3 resonance.

The field equation for $\phi^\alpha(\mathbf{x},t)$ is still

$$[\Box-\mu^2-\lambda\phi^\beta\phi^\beta+\beta\theta(a-x)]\phi^\alpha =-(G/2m)\nabla\cdot[\tau^\alpha\boldsymbol{\sigma}S(x)]. \quad \text{(B1)}$$

The nucleon source distribution $S(x)$ was introduced by making the identification (4.6):

$$\psi^\dagger\boldsymbol{\sigma}\tau_\alpha\psi\rightarrow S(x)\boldsymbol{\sigma}\tau_\alpha$$

in the standard field theory. Using the anticommutation relations for the nucleon fields in this standard theory, we find

$$\begin{aligned}&[\psi^\dagger(\mathbf{x}')\tau_\alpha\psi(\mathbf{x}'),\psi^\dagger(\mathbf{x})\tau_\beta\psi(\mathbf{x})]\\ &\qquad=\delta^{(3)}(\mathbf{x}-\mathbf{x}')\psi^\dagger(\mathbf{x})2i\epsilon_{\alpha\beta\gamma}\tau_\gamma\psi(\mathbf{x}),\\ &[\psi^\dagger(\mathbf{x}')\sigma_\alpha\psi(\mathbf{x}'),\psi^\dagger(\mathbf{x})\sigma_\beta\psi(\mathbf{x})]\\ &\qquad=\delta^{(3)}(\mathbf{x}-\mathbf{x}')\psi^\dagger(\mathbf{x})2i\epsilon_{\alpha\beta\gamma}\sigma_\gamma\psi(\mathbf{x}).\end{aligned} \quad \text{(B2)}$$

Now,

$$\begin{aligned}&\frac{\partial}{\partial t}[\psi^\dagger(\mathbf{x})\tau_\alpha\psi(\mathbf{x})]=i[H,\psi^\dagger(\mathbf{x})\tau_\alpha\psi(\mathbf{x})],\\ &\frac{\partial}{\partial t}[\psi^\dagger(\mathbf{x})\sigma_\alpha\psi(\mathbf{x})]=i[H,\psi^\dagger(\mathbf{x})\sigma_\alpha\psi(\mathbf{x})].\end{aligned} \quad \text{(B3)}$$

Using the commutation relations (B2) and the Hamiltonian given in Eq. (4.1), we have

$$\begin{aligned}\frac{\partial}{\partial t}[\psi^\dagger(\mathbf{x})\tau_\alpha\psi(\mathbf{x})]&=-\frac{G}{m}\psi^\dagger(\mathbf{x})[\boldsymbol{\tau}\times(\boldsymbol{\sigma}\cdot\boldsymbol{\nabla})\boldsymbol{\phi}]_\alpha\psi(\mathbf{x}),\\ \frac{\partial}{\partial t}[\psi^\dagger(\mathbf{x})\sigma_\alpha\psi(\mathbf{x})]&=-\frac{G}{m}\psi^\dagger(\mathbf{x})[\boldsymbol{\tau}\cdot(\boldsymbol{\sigma}\times\boldsymbol{\nabla})_\alpha\boldsymbol{\phi}]\psi(\mathbf{x}).\end{aligned}\tag{B4}$$

Making the identification of the time-independent source function $S(x)$, we obtain

$$\begin{aligned}\dot\tau_\alpha S(x)&=-(G/m)S(x)\sigma_\kappa[\boldsymbol{\tau}\times\nabla_\kappa\boldsymbol{\phi}]_\alpha{}^{\mathrm{sym}},\\ \dot\sigma_\alpha S(x)&=-(G/m)S(x)\tau_\kappa[\boldsymbol{\sigma}\times\boldsymbol{\nabla}\boldsymbol{\phi}_\kappa]_\alpha{}^{\mathrm{sym}}.\end{aligned}\tag{B5}$$

We have again symmetrized the equations since this changes nothing in the correct theory. The Eqs. (B1) and (B5) constitute the coupled equations.[16] If we take the current $\hat{\mathbf{J}}$ as given in Eq. (4.7) and use the coupled equations to compute $\nabla\cdot\hat{\mathbf{J}}\equiv-\dot\rho$, we find

$$\dot\rho=\frac{\partial}{\partial t}\left[\boldsymbol{\phi}\times\frac{\partial\boldsymbol{\phi}}{\partial t}\right]_3^{\mathrm{sym}}-\frac{G}{2m}S(x)\sigma_\kappa[\boldsymbol{\tau}\times\nabla_\kappa\boldsymbol{\phi}]_3{}^{\mathrm{sym}}.\tag{B6}$$

(We have again assumed that $[\phi_\beta\phi_\beta,\phi_\alpha]=0$.) It then follows immediately that

$$\hat\rho=[\boldsymbol{\phi}\times\partial\boldsymbol{\phi}/\partial t]_3{}^{\mathrm{sym}}+S(x)\tfrac{1}{2}(1+\tau_3).\tag{B7}$$

Thus, the system of coupled equations formally yields the same expressions for $\hat{\mathbf{J}}$ and $\dot\rho$ as does the standard theory [see Eqs. (4.7)].

Although the derivation may leave something to be desired, the reader can consider Eqs. (B1) and (B5) together with (B6) and (4.18) as the set of coupled equations of motion, together with a conserved current, which define the model.

Now let us consider excitations about the ground state. As before, we write

$$\phi^\alpha(\mathbf{x},t)=\phi_0{}^\alpha(\mathbf{x})+\eta^\alpha(\mathbf{x},t).$$

We also expand τ^α and σ^α about ground-state values:

$$\tau^\alpha=\tau_0{}^\alpha+\delta\tau^\alpha,\quad \sigma^\alpha=\sigma_0{}^\alpha+\delta\sigma^\alpha.\tag{B8}$$

The zeroth-order equations are then

$$\begin{aligned}[\nabla^2-\mu^2-\lambda\phi_0{}^\beta\phi_0{}^\beta+\beta\theta(a-x)]\phi_0{}^\alpha(\mathbf{x})&\\ =-(G/2m)\tau_0{}^\alpha(\boldsymbol{\sigma}_0\cdot\boldsymbol{\nabla})S(x),&\\ \dot\tau_0{}^\alpha S(x)=-(G/m)S(x)\sigma_0{}^\kappa[\boldsymbol{\tau}_0\times\nabla_\kappa\boldsymbol{\phi}_0]_\alpha{}^{\mathrm{sym}},&\\ \dot\sigma_0{}^\alpha S(x)=-(G/m)S(x)\tau_0{}^\kappa[\boldsymbol{\sigma}_0\times\boldsymbol{\nabla}\phi_0{}^\kappa]_\alpha{}^{\mathrm{sym}}.&\end{aligned}\tag{B9}$$

$S(x)$ vanishes for $x>a$. Thus it is consistent to take $\dot\tau_0{}^\alpha=0=\dot\sigma_0{}^\alpha$ for $x>a$. For $x<a$, the variational form for $\phi_0{}^\alpha$ is, from (3.9),

$$\phi_0{}^\alpha(\mathbf{x})=\phi_0(x)\tau_0{}^\alpha(\boldsymbol{\sigma}_0\cdot\hat{x}).\tag{B10}$$

It then follows that

$$[\boldsymbol{\tau}_0\times\nabla_i\boldsymbol{\phi}_0]_\alpha{}^{\mathrm{sym}}=0=[\boldsymbol{\sigma}_0\times\boldsymbol{\nabla}\phi_0{}^i]_\alpha{}^{\mathrm{sym}},\tag{B11}$$

where we have used the result

$$\boldsymbol{\nabla}(\boldsymbol{\sigma}\cdot\hat{x})=\frac{\boldsymbol{\sigma}}{x}-\frac{\hat{x}}{x}(\boldsymbol{\sigma}\cdot\hat{x})\tag{B12}$$

in deriving the second equality. The conclusion follows that it is consistent with the coupled equations to take $\dot\tau_0{}^\alpha=0=\dot\sigma_0{}^\alpha$.

We next consider the first-order (in η^α, $\delta\tau^\alpha$ and $\delta\sigma^\alpha$) coupled equations. They are

$$\begin{aligned}[\Box-\mu^2-\lambda\phi_0{}^\beta\phi_0{}^\beta+\beta\theta(a-x)]\eta^\alpha&=\lambda\eta^\beta[\phi_0{}^\alpha\phi_0{}^\beta+\phi_0{}^\beta\phi_0{}^\alpha]\\ &-(G/2m)[\boldsymbol{\sigma}_0\cdot\boldsymbol{\nabla}(\delta\tau^\alpha S(x))+\tau_0{}^\alpha\boldsymbol{\nabla}\cdot(\boldsymbol{\delta\sigma}S(x))],\end{aligned}\tag{B13}$$

$$\begin{aligned}\delta\dot\tau^\alpha S(x)&=-(G/m)S(x)\sigma_0{}^\kappa\\ &\quad\times[(\boldsymbol{\delta\tau}\times\nabla_\kappa\boldsymbol{\phi}_0)_\alpha{}^{\mathrm{sym}}+(\boldsymbol{\tau}_0\times\nabla_\kappa\boldsymbol{\eta})_\alpha{}^{\mathrm{sym}}],\\ \delta\dot\sigma^\alpha S(x)&=-(G/m)S(x)\tau_0{}^\kappa\\ &\quad\times[(\boldsymbol{\delta\sigma}\times\boldsymbol{\nabla}\phi_0{}^\kappa)_\alpha{}^{\mathrm{sym}}+(\boldsymbol{\sigma}_0\times\boldsymbol{\nabla}\eta^\kappa)_\alpha{}^{\mathrm{sym}}].\end{aligned}\tag{B14}$$

In deriving the last two equations we have used the results of Eq. (B11). Suppose that we can neglect the first term in each of Eqs. (B14). Then $\delta\tau^\alpha$ must have the form

$$\delta\tau^\alpha(\mathbf{x},t)=\delta\tau^\alpha(\mathbf{x})e^{-i\omega t},\tag{B15}$$

and Eq. (B14) becomes

$$i\omega\delta\tau^\alpha(\mathbf{x})\approx(G/m)\sigma_0{}^\kappa[\boldsymbol{\tau}_0\times\nabla_\kappa\boldsymbol{\eta}(\mathbf{x})]_\alpha{}^{\mathrm{sym}}.\tag{B16}$$

To see if this approximation is valid, we must estimate the magnitudes of the two terms in Eq. (B14). Define the quantity γ by

$$\gamma\equiv\frac{|\boldsymbol{\delta\tau}\times\nabla_i\boldsymbol{\phi}_0|}{|\boldsymbol{\tau}_0\times\nabla_i\boldsymbol{\eta}|}\approx\frac{|\delta\tau||\nabla_i\phi_0|}{|\boldsymbol{\tau}_0\times\nabla_i\boldsymbol{\eta}|}.\tag{B17}$$

Using Eq. (B16) for $|\delta\tau|$, we have

$$\gamma\approx\frac{1}{\omega}\frac{G}{m}|\sigma_0||\nabla_i\phi_0|\approx\frac{\mu}{\omega}\frac{\mu}{m}G\frac{(ca)}{(\mu a)^2}.\tag{B18}$$

In terms of the parameter α defined in Eq. (3.26),

$$\gamma=2\alpha\frac{\mu}{\omega}\frac{(\mu a)(ca)^2}{(\mu a)^2}.$$

Using the values of $(\mu a)(ca)^2$ determined from the fits to the inelastic form factors in Sec. 6, we have the following representative results:

State	γ
$\frac{3}{2}+,\frac{3}{2}$ (1236)	0.61
$\frac{3}{2}-,\frac{1}{2}$ (1512)	0.059
$\frac{5}{2}+,\frac{1}{2}$ (1688)	0.047

Thus, for the higher resonances $\gamma \ll 1$, and our approximation proves to be excellent. [Because of the factor $1/\omega$ in Eq. (B18) the approximation becomes even better as the mass of the resonance increases.] For the 3-3 resonance the approximation is only fair. The reason for the large value of γ here is that we need a larger value of c to fit the experimental data than for the other resonances. Thus, with the possible exception of the low-lying 3-3 resonance, we can write

$$\begin{aligned}\delta\dot{\tau}^\alpha S(x) &\approx -(G/m)S(x)\sigma_0{}^\kappa[\tau_0\times\nabla_\kappa\boldsymbol{\eta}]_\alpha{}^{\mathrm{sym}},\\ \delta\dot{\sigma}^\alpha S(x) &\approx -(G/m)S(x)\tau_0{}^\kappa[\boldsymbol{\sigma}_0\times\boldsymbol{\nabla}\eta^\kappa]_\alpha{}^{\mathrm{sym}}.\end{aligned} \tag{B19}$$

The coupled equations thus give

$$\begin{aligned}\dot{\rho}\approx{}&[\boldsymbol{\phi}_0\times\partial^2\boldsymbol{\eta}/\partial t^2]_3\\ &-(G/2m)S(x)\sigma_0{}^\kappa[\tau_0\times\nabla_\kappa\boldsymbol{\eta}]_\alpha{}^{\mathrm{sym}}.\end{aligned} \tag{B20}$$

Interpreting $\boldsymbol{\sigma}_0$ and τ_0 as our original time-independent vectors, we note that this result is the same as that of Eqs. (4.10) and (4.20). Thus, we see that Eqs. (4.10) and (4.20) for $\dot{\rho}$ already contain the leading term from $\dot{\tau}$. We conclude, therefore, that if one were to solve the coupled equations (B1) and (B5), the resulting current and charge density would not differ greatly from those we have computed by setting $\dot{\tau}=\dot{\sigma}=0$. We can also show that the terms involving $\delta\tau$ and $\delta\sigma$ in the field equation (B13) for η^α are small compared to the $(\beta a^2-5\lambda c^2a^2)$ term. Hence, Eq. (3.12) would not be modified significantly if one solved the set of coupled equations. Defining

$$\gamma'\equiv\frac{|(G/2m)\boldsymbol{\nabla}\cdot[\boldsymbol{\sigma}_0\delta\tau^\alpha S(x)+\tau_0{}^\alpha\delta\boldsymbol{\sigma}S(x)]|}{|[\beta-5\lambda c^2]\boldsymbol{\eta}|}, \tag{B21}$$

we find

$$\gamma'\approx\left(\frac{\mu G}{m}\right)^2\frac{\mu}{\omega}\frac{1}{(\mu a)^3}\frac{1}{(\beta a^2-5\lambda c^2a^2)}. \tag{B22}$$

Representative values are as follows:

State	γ'
$\frac{3}{2}+,\frac{3}{2}$ (1236)	0.76
$\frac{3}{2}-,\frac{1}{2}$ (1512)	0.074
$\frac{5}{2}+,\frac{1}{2}$ (1688)	0.059

Again with the exception of the 3-3 resonance, $\gamma'\ll 1$, and we conclude that the modifications arising from the coupled equations would be small.